

2

DTIC FILE

# HTMIAC

A Department of Defense Information Analysis Center

AD-A217 193

## FAILURE MECHANISMS OF COMPOSITE STRUCTURES

S. R. Soni, S. C. Tan, G. P. Tandon, T. Hsiao, L. Roundy,  
Barbara Woolsey, and Lisa Wilson  
(AdTech Systems Research Inc.)

DTIC  
SELECTE  
JAN 05 1990  
S D D

Final Technical Report  
to  
AIR FORCE WRIGHT RESEARCH AND DEVELOPMENT CENTER  
Materials Laboratory  
ATTN: WRDC/MLBM  
Wright-Patterson Air Force Base, Ohio 45433-6533

HTMIAC Report 17

Defense Electronics Supply Center Contract No. DLA900-86-C-0751

September 1989

"Approved for public release; distribution is unlimited."

90 01 05 006

HIGH TEMPERATURE MATERIALS - MECHANICAL, ELECTRONIC AND THERMOPHYSICAL  
PROPERTIES INFORMATION ANALYSIS CENTER

Operated by  
CENTER FOR INFORMATION AND NUMERICAL DATA ANALYSIS AND SYNTHESIS  
PURDUE UNIVERSITY  
2595 YEAGER ROAD  
WEST LAFAYETTE, INDIANA 47906

REPORT DOCUMENTATION PAGE			Form Approved OMB No. 0704-0188	
Public reporting burden for this collection of information is estimated to average 1 hour per response, including the time for reviewing instructions, searching existing data sources, gathering and maintaining the data needed, and completing and reviewing the collection of information. Send comments regarding this burden estimate or any other aspect of this collection of information, including suggestions for reducing this burden, to Washington Headquarters Services, Directorate for Information Operations and Reports, 1215 Jefferson Davis Highway, Suite 1204, Arlington, VA 22202-4302, and to the Office of Management and Budget, Paperwork Reduction Project (0704-0188), Washington, DC 20503				
1. AGENCY USE ONLY (Leave blank)	2. REPORT DATE September 1989	3. REPORT TYPE AND DATES COVERED Final Technical Report		
4. TITLE AND SUBTITLE Failure Mechanisms of Composite Structures			5. FUNDING NUMBERS Defense Electronics Supply Center Contract Number: DLA900-86-C-0751 Air Force WRDC/Materials Laboratory MIPR No.: FY1457-87-N-5057 Amendment 01	
6. AUTHOR(S) S.R. Soni, S.C. Tan, G.P. Tandon, T. Hsiao, L. Roundy, Barbara Woolsey, and Lisa Wilson (AdTech Systems Research Inc.)			8. PERFORMING ORGANIZATION REPORT NUMBER  HTMIAC Report 17	
7. PERFORMING ORGANIZATION NAME(S) AND ADDRESS(ES) High Temperature Materials - Mechanical, Electronic and Thermophysical Properties Information Analysis Center CINDAS/Purdue University (HTMIAC) 2595 Yeager Road West Lafayette, Indiana 47906			10. SPONSORING/MONITORING AGENCY REPORT NUMBER	
9. SPONSORING/MONITORING AGENCY NAME(S) AND ADDRESS(ES) Air Force Wright Research and Development Center Materials Laboratory, ATTN: WRDC/MLBM, Wright-Patterson Air Force Base, Ohio 45433-6533 Office of the Director of Defense Research & Engineering (Research & Advanced Technology), Pentagon, Washington, DC			11. SUPPLEMENTARY NOTES DC 20301-3080	
11. SUPPLEMENTARY NOTES Hard copies available from HTMIAC (price \$45.00); DTIC assigned HTMIAC Source Code: 413571				
12a. DISTRIBUTION / AVAILABILITY STATEMENT Approved for public release; distribution is unlimited.			12b. DISTRIBUTION CODE	
13. ABSTRACT (Maximum 200 words) This Final Technical Report contains details of technical work accomplished and results obtained in the performance of HTMIAC Special Study Item 0001AE: "Prediction of Failure Mechanisms and Repair of Damages of Composite Aircraft Structures." Because only a small portion of the funding for the Special Study was actually awarded, this Special Study was performed only partially. Nevertheless, this report contains detailed results of the following completed research works:  <ul style="list-style-type: none"> <li>(1) Mixed-Mode Fracture of Notched Unidirectional and Off-Axis Laminates under Tensile Loading.</li> <li>(2) Thermo-Elastic Model for Multidirectional Coated Fiber Composites: Traction Formulation.</li> <li>(3) Constrained Matrix Cracking.</li> </ul>				
14. SUBJECT TERMS Composite structure, composite laminate, graphite/epoxy composites, Nicalon/BMAS composites, failure mechanisms, failure prediction, mechanical properties.			15. NUMBER OF PAGES 84	
			16. PRICE CODE	
17. SECURITY CLASSIFICATION OF REPORT UNCLASSIFIED	18. SECURITY CLASSIFICATION OF THIS PAGE UNCLASSIFIED	19. SECURITY CLASSIFICATION OF ABSTRACT UNCLASSIFIED	20. LIMITATION OF ABSTRACT UNLIMITED	

## PREFACE

This Final Technical Report contains details of technical work accomplished and results obtained in the performance of HTMIAC Special Study Item 0001AE: "Prediction of Failure Mechanisms and Repair of Damages of Composite Aircraft Structures." Because only a small portion of the funding for the Special Study was actually awarded, this Special Study was performed only partially. Nevertheless, this report contains detailed results of the following completed research works:

- (1) Mixed-Mode Fracture of Notched Unidirectional and Off-Axis Laminates under Tensile Loading.
- (2) Thermo-Elastic Model for Multidirectional Coated Fiber Composites: Traction Formulation.
- (3) Constrained Matrix Cracking.

This Special Study was supported by the Air Force Wright Research and Development Center (WRDC), Materials Laboratory, ATTN: WRDC/MLBM (Mechanics and Surface Interactions Branch), Wright-Patterson Air Force Base, Ohio 45433-6533. It was funded through WRDC/Materials Laboratory MIPR No. FY1457-87-N-5057 Amendment 01. The Air Force Program Manager was Dr. Stephen W. Tsai. In performing this Special Study, HTMIAC collaborated with its subcontractor: AdTech Systems Research Inc., 1342 North Fairfield Road, Dayton, Ohio 45432-2698.

HTMIAC is a U.S. Department of Defense Information Analysis Center sponsored by the Office of the Director of Defense Research and Engineering (Research and Advanced Technology), Pentagon, Washington, DC 20301-3080. HTMIAC is operated by the Center for Information and Numerical Data Analysis and Synthesis (CINDAS), Purdue University, West Lafayette, Indiana 47906, under the Defense Logistics Agency (DLA) Contract DLA900-86-C-0751. The DLA contract is awarded to Purdue by the Defense Electronics Supply Center, Dayton, Ohio 45444-5208, with Ms. Sara M. Williams as the Contracting Officer.

HTMIAC is under the technical direction of Mr. Jerome Persh, Office of the Director of Defense Research and Engineering (Research and Advanced Technology), Attn: ODDR&E (R&AT/ET), Pentagon, Room 3D1089, Washington, D.C. 20301-3080 and Mr. Roger E. Rondeau, Air Force Wright Research and Development

Center, Attn: WRDC/MLPJ, Wright-Patterson Air Force Base, Ohio 45433-6533. HTMIAC is under the IACs program management of Mr. Paul M. Klinefelter and Mr. Brian P. McCabe, the Defense Technical Information Center (DTIC), Attn: DTIC-DF, Cameron Station, Alexandria, Virginia 22304-6145.

HTMIAC serves as the DoD's central source of data and information on high temperature materials properties, especially the properties of aerospace structural composites and metals and infrared detector/sensor materials. It supports the DoD research, development, test, evaluation, engineering, and studies programs as well as weapons systems and military hardware in general, and supports the DoD Tri-Service Laser Hardened Materials and Structures Group (LHMSG) to meet the material property data requirements for high energy laser structural and detector/sensor vulnerability, survivability, and hardening assessments and studies in particular. It also provides similar support to the DoD high energy laser community associated with the Strategic Defense Initiative (SDI) programs.

To fulfill its assigned mission to support the DoD, HTMIAC performs both its basic operations and special studies/tasks. The work detailed in this final technical report constitutes one of the special studies of HTMIAC.

Accession For	
NTIS CRA&I	<input checked="" type="checkbox"/>
DTIC TAB	<input type="checkbox"/>
Unannounced	<input type="checkbox"/>
Justification	
By 45.00-HTMIAC	
Distribution/	
Availability Codes	
Dist	Avail and/or Special
A-1	24

C. Y. Ho  
 Director  
 HTMIAC and CINDAS



## TABLE OF CONTENTS

	<u>Page</u>
REPORT DOCUMENTATION PAGE (Standard Form 298) . . . . .	i
PREFACE . . . . .	iii
LIST OF TABLES . . . . .	vii
LIST OF FIGURES . . . . .	viii
I. MIXED-MODE FRACTURE OF NOTCHED UNIDIRECTIONAL AND OFF-AXIS LAMINATES UNDER TENSILE LOADING . . . . .	1
Abstract . . . . .	2
1. Introduction . . . . .	3
2. Stress Analysis . . . . .	3
3. Complex Roots . . . . .	5
4. Failure Models . . . . .	6
4.1. Point Strength Model (PSM) . . . . .	7
4.2. Minimum Strength Model (MSM) . . . . .	7
5. Finite-Width Correction Factors . . . . .	8
6. Experiment and Results . . . . .	8
6.1. Procedures . . . . .	8
6.2. Failure Mechanism . . . . .	9
6.3. Notched Strength . . . . .	9
7. Correlation of Theory with Experiment . . . . .	10
7.1. Characteristic Length as a Constant . . . . .	10
7.2. Characteristic Length as a Power Function . . . . .	11
8. Discussions and Conclusion . . . . .	12
Acknowledgement . . . . .	13
References . . . . .	13
II. THERMO-ELASTIC MODEL FOR MULTIDIRECTIONAL COATED FIBER COMPOSITES: TRACTION FORMULATION . . . . .	27
Abstract . . . . .	28
1. Introduction . . . . .	29
2. The Composite Model . . . . .	31
3. Boundary Value Problem . . . . .	32
4. General Solution . . . . .	36
5. The Composite Response . . . . .	39
6. Numerical Results and Discussion . . . . .	40
7. The NDSANDS Program . . . . .	44

8.	Summary . . . . .	45
	References . . . . .	45
	Appendix . . . . .	48
III.	CONSTRAINED MATRIX CRACKING . . . . .	59
1.	Introduction . . . . .	60
2.	Analytical Model . . . . .	60
3.	Results and Discussion . . . . .	63
4.	Conclusions . . . . .	74
	References . . . . .	74

## LIST OF TABLES

	<u>Page</u>
<u>Section I</u>	
1a. Elastic Properties of the Graphite/Epoxy AS4/3502 Lamina . . . . .	16
1b. Strength Properties of the Graphite/Epoxy AS4/3502 Lamina . . . . .	16
2. Experimental Results for the Graphite/Epoxy AS4/3502 [0g] Lamina Containing a Circular Hole or a Central Crack . . . . .	16
3. Experimental Results for the Gr/Ep AS4/3502: (a) [ <u>+</u> 30 <sub>2</sub> ] <sub>s</sub> , (b) [ <u>+</u> 45 <sub>2</sub> ] <sub>s</sub> , (c) [ <u>+</u> 60 <sub>2</sub> ] <sub>s</sub> Laminates with a Circular Hole . . . . .	17
4. Experimental Results for the Gr/Ep AS4/3502: (a) [ <u>+</u> 30 <sub>2</sub> ] <sub>s</sub> , (b) [ <u>+</u> 45 <sub>2</sub> ] <sub>s</sub> , (c) [ <u>+</u> 60 <sub>2</sub> ] <sub>s</sub> Laminates with a Center Crack . . . . .	18
<u>Section II</u>	
1. Effective Elastic Properties for Unidirectional Graphite/ Epoxy and Nicalon/BMAS Composite Systems . . . . .	53
2. Effective Thermo-Elastic Moduli for Three-Directional 'Isotropic' Composite . . . . .	53
3a. Stress Component $\sigma_r$ in the Fiber-Coating and Coating-Matrix Interface for $\Delta T = -1^\circ C$ . . . . .	54
3b. Stress Component $\sigma_\theta$ (algebraic maximum) in the Fiber, Coating and Matrix for $\Delta T = -1^\circ C$ . . . . .	54
3c. Stress Component $\sigma_z$ in the Fiber, Coating and Matrix for $\Delta T = -1^\circ C$ . . . . .	55
<u>Section III</u>	
1. Specimen Dimensions for Doubling the Failure Strain . . . . .	75

LIST OF FIGURES

	<u>Page</u>
<u>Section I</u>	
1. Coordinates System of an Infinite Composite Laminate Containing an Opening . . . . .	19
2. Tangential Stress Distribution, $\sigma_{\theta}$ , at Various Characteristic Curves of a Graphite/Epoxy $[\pm 45]_S$ Laminate with a Circular Hole . . . . .	19
3. The Characteristic Length $b_1$ , Used for the Point Strength Model, Is Measured along the Assumed Fracture Propagating Plane . . . . .	20
4. Finite-Width Correction Factors for AS4/3502 $[\pm 0]_S$ Laminates and Isotropic Plate with a Central Hole . . . . .	20
5. Failed Patterns of the Gr/Ep AS4/3502 $[\pm 30]_S$ (left) and $[\pm 60]_S$ (right) Laminates with a Circular Hole . . . . .	21
6. Failed Patterns of the Gr/Ep AS4/3502 $[\pm 30]_S$ (left) and $[\pm 60]_S$ (right) Containing a Central Crack . . . . .	21
7. Comparison of the Predicted Notched Strength (MSM) and the Experimental Data for the $[\pm 0]_S$ Laminates with a Central Hole . . . . .	22
8. Gross Strength Reduction Factor and Magnitude versus Opening-to-Width Ratio for the $[\pm 0]_S$ Laminates with a Central Hole . . . . .	23
9. Correlation of the Predicted Strength (PSM and MSM) and the Experimental Data for the $[\pm 0]_S$ Laminates Containing a Central Crack . . . . .	24
10. Experimental Data and Predicted Notched Strength Using a Modified $b_0$ (MSM) for the $[\pm 45]_S$ Laminate . . . . .	25
11. Experimental Data and Predicted Notched Strength Using a Modified $b_0$ (MSM) for the $[\pm 60]_S$ Laminate . . . . .	25
12. Predicted Gross Strength Reduction Factor and Magnitude as a Function of the Opening-to-Width Ratio for the $[\pm 0]_S$ Laminates with a Central Crack . . . . .	26
<u>Section II</u>	
1. Theoretical Model . . . . .	56
2. (a) Composite (b) Equivalent Homogeneous Body . . . . .	57

3. Effective Thermal Expansion Coefficients for (a) Graphite/Epoxy System (b) Nicalon/BMAS System . . . . .	58
--	----

Section III

1. Centrally Cracked Strip with Stiffened Edge . . . . .	61
2. Effect of Stringers on Strain Energy Release Rate . . . . .	64
3. Effect of Stringers on Strain Energy Release Rate . . . . .	65
4. Effect of Stringer Size on Inherent Flaw Growth . . . . .	67
5. Matrix Cracking Stress . . . . .	68
6. Effect of Spacing on Crack Initiation and Growth . . . . .	70
7. Effect of Spacing on Crack Initiation and Growth . . . . .	71
8. Effect of Spacing on Crack Initiation and Growth . . . . .	72
9. Effect of Stringer Thickness on Cracking Strain . . . . .	73

**SECTION I**

**MIXED-MODE FRACTURE OF NOTCHED  
UNIDIRECTIONAL AND OFF-AXIS LAMINATES  
UNDER TENSILE LOADING**

## ABSTRACT

The mixed-mode fracture of matrix dominated composite laminates containing central holes and cracks was studied using some graphite/epoxy off-axis AS4/3502 balanced symmetric laminates,  $[\pm\phi_2]_S$ . The uniaxial failure of a  $0^\circ$  laminate, which is the main load carrier of multidirectional laminates, was also investigated. Interesting results were observed for the  $[\pm\phi_2]_S$  laminates with a central normal crack. In this paper, the terms "notch sensitivity" and the "notched shape sensitivity" are distinguished, defined and classified with examples. Anisotropic finite width correction factors were applied to interpolate the experimental data. In general, the predicted notched strength and the failure initiation locations correlate reasonably well with the experimental results.

## 1. INTRODUCTION

Mixed-mode fracture in composite laminates has been an interesting subject since it involves several stresses and strength components as well as their interactions. In the case of composite laminates containing stress concentrations, the failure analysis can be performed using the stress state at a point or using the average stress along a characteristic distance. These have been well documented in the literature under mode I failure condition.

The failure of composite materials can basically be classified into fiber dominated mode and matrix dominated mode. The mixed-mode fracture of fiber dominated composite laminates containing stress concentrations has been studied by Morris and Hahn [1] under a uniaxial tensile loading and by the present author [2] under a uniaxial and combined in-plane loading conditions. The former analysis was based on laminate stress whereas the later was based on ply-by-ply level stresses. Good correlation between theory and experimental data has generally been obtained in Ref. [2]. Very few research has been reported for the failure of matrix dominated composite laminates containing stress concentrations. Mar and Lin [3] investigated experimentally the fracture strength of boron/aluminum  $[\pm 45]_{2s}$  laminate with a central circular opening. Recently, Chang and Chang [4] utilized a progressive failure model to predict the strength of two matrix dominated laminates with a central hole. Other relevant work may be found from a review by Awerbuch and Madhukar [5]. In addition to the matrix dominated composite laminates, the failure of unidirectional  $0^\circ$  laminates with stress concentrations is also an important subject.

In this paper, an experimental program using the graphite/epoxy AS4/3502 off-axis symmetric laminates,  $[\pm\phi_2]_s$ , containing either a circular hole or a central crack was designed to study the mixed-mode failure mechanism and fracture strength of matrix dominated composite laminates under tensile loading. The point strength model and the minimum strength model [6] were applied to correlate the experimental results with theory. The failure of  $[0_8]$  laminates with through-the-thickness holes and cracks were also investigated. From this study, the term "notch sensitivity", normally used by people, can be classified into "notch sensitivity" and "notched shape sensitivity". They can be defined and distinguished remarkably utilizing the result of the present experimental data.

## 2. STRESS ANALYSIS

The stress distribution of infinite anisotropic plates containing an elliptical opening has been derived earlier [2, 6] under in-plane combined loading condition. The

coordinates system of a laminate subjected to uniaxial loading is illustrated in Figure 1. In the case that an orthotropic laminate is symmetric with respect to its mid-plane, the extensional and bending stiffnesses are uncoupled. Using Lekhnitskii's complex potentials [7], the stresses, given in the principal coordinates of the opening (1-2 axes), were obtained in the following

$$\begin{aligned}\sigma_1 &= 2 \operatorname{Re} [\mu_1^2 \phi_1'(z_1) + \mu_2^2 \phi_2'(z_2)] \\ \sigma_2 &= 2 \operatorname{Re} [\phi_1'(z_1) + \phi_2'(z_2)] \\ \sigma_6 &= -2 \operatorname{Re} [\mu_1 \phi_1'(z_1) + \mu_2 \phi_2'(z_2)]\end{aligned}\quad (1)$$

where  $\phi_1'$  and  $\phi_2'$  denote the derivatives of the complex potentials  $\phi_1$  and  $\phi_2$  with respect to  $z_1$  and  $z_2$  respectively, and

$$\begin{aligned}\phi_1(z_1) &= \frac{\beta_1 - \mu_2 \alpha_1}{\mu_1 - \mu_2} \frac{1}{\zeta_1} \\ \phi_2(z_2) &= \frac{\beta_1 - \mu_1 \alpha_1}{\mu_1 - \mu_2} \frac{1}{\zeta_2}\end{aligned}\quad (2)$$

where

$$\alpha_1 = -(\sigma_x/2) \cos \psi (\operatorname{acos} \psi + i \operatorname{bsin} \psi) \quad (3)$$

$$\beta_1 = -(\sigma_x/2) \sin \psi (\operatorname{acos} \psi + i \operatorname{bsin} \psi)$$

and

$$\zeta_i = \frac{z_i + \sqrt{z_i^2 - a^2 - \mu_i^2 b^2}}{a - i \mu_i b}, \quad i = 1, 2 \quad (4)$$

$$z_i = x' + \mu_i y'$$

where  $x'$  and  $y'$  are along the principal axes of the opening, i.e., 1 and 2 axes, respectively. The parameters  $\mu_1$  and  $\mu_2$  are the complex roots of the characteristic equation

$$a_{11} \mu^4 - 2a_{16} \mu^3 + (2a_{12} + a_{66}) \mu^2 - 2a_{26} \mu + a_{22} = 0 \quad (5)$$

where  $a_{ij}$ ,  $i, j = 1, 2, 6$ , are the components of the compliance matrix of the anisotropic laminate.

The stress analysis is pursued using a superposition technique. The solution is given in index notation as:

$$\sigma_i = \sigma_i^o + \sigma_i^*, \quad i = 1, 2, 6 \quad (6)$$

where  $\sigma_i$  denotes the local laminate stress; the parameters  $\sigma_i^{\circ}$  and  $\sigma_i^*$  are the stress components due to the uniform stress field and the opening, respectively. The solution of these stress components has been obtained in closed form in References [2, 6, 10]. In the above equations,  $a$  and  $b$  are the semi-major and semi-minor axes of the elliptical opening respectively. The parameter  $b_o$ , Figure 1, denotes a characteristic length between the characteristic curve and the opening contour, and  $\theta$  is the angle between the 1-axis and the normal vector of the characteristic curve. In addition,  $\psi$  designates the slanted angle of the elliptical opening measured from the y-axis.

The tangential stress along the characteristic curve can be obtained using the stress transformation rule as

$$\sigma_{\theta} = \{\sigma_1(a + b_o)^2 \sin^2 \theta + \sigma_2(b + b_o)^2 \cos^2 \theta - 2\sigma_6(a + b_o)(b + b_o) \sin \theta \cos \theta\} / \gamma^2 \quad (7)$$

where

$$\gamma^2 = (a + b_o)^2 \sin^2 \theta + (b + b_o)^2 \cos^2 \theta \quad (8)$$

### 3. COMPLEX ROOTS

In the case of orthotropic laminate,  $a_{16} = a_{26} = 0$ , the characteristic equation, Equation (5), reduces to

$$a_{11}\mu^4 + (2a_{12} + a_{66})\mu^2 + a_{22} = 0 \quad (9)$$

Equation (9) has been solved analytically by the present author [8]. In this section, the complex roots are solved using a different method, which is probably simpler than the earlier one. Between the two principal roots the following relationship exists [7]:

$$\begin{aligned} \mu_1 \mu_2 &= -\sqrt{\frac{a_{22}}{a_{11}}} \\ i(\mu_1 + \mu_2) &= -\sqrt{\frac{2a_{12} + a_{66}}{a_{11}}} + 2\sqrt{\frac{a_{22}}{a_{11}}} \end{aligned} \quad (10)$$

In terms of engineering properties, these equations can be rewritten as:

$$\begin{aligned} \mu_1 \mu_2 &= -\sqrt{\frac{E_x}{E_y}} \\ \mu_1^2 + \mu_2^2 &= 2\nu_{xy} - \frac{E_x}{G_{xy}} \end{aligned} \quad (15)$$

$$i(\mu_1 + \mu_2) = - \sqrt{\frac{E_x}{G_{xy}} - 2\nu_{xy} + 2\sqrt{\frac{E_x}{E_y}}} + \sqrt{\frac{E_x}{G_{xy}} - 2\nu_{xy} - 2\sqrt{\frac{E_x}{E_y}}}$$

where  $E_x$ ,  $E_y$  and  $G_{xy}$  are the laminate extensional and shear moduli, respectively, and  $\nu_{xy}$  denotes the effective laminate Poisson's ratio.

The two principal complex roots,  $\mu_1$  and  $\mu_2$ , can be solved using Equation (11). The solution is

$$\mu_1 = \frac{i}{2} \left[ \sqrt{\frac{E_x}{G_{xy}} - 2\nu_{xy} + 2\sqrt{\frac{E_x}{E_y}}} + \sqrt{\frac{E_x}{G_{xy}} - 2\nu_{xy} - 2\sqrt{\frac{E_x}{E_y}}} \right] \quad (12)$$

$$\mu_2 = \frac{i}{2} \left[ \sqrt{\frac{E_x}{G_{xy}} - 2\nu_{xy} + 2\sqrt{\frac{E_x}{E_y}}} - \sqrt{\frac{E_x}{G_{xy}} - 2\nu_{xy} - 2\sqrt{\frac{E_x}{E_y}}} \right]$$

Substituting Equation (12) into Equations (1-8), we obtain the stresses in the principal axes of the opening as well as the tangential stress along the characteristic curve. As an example, the tangential stress of a graphite/epoxy  $[\pm 45_2]_S$  laminate was generated in Figure 2 along different characteristic curves. The material properties are given in Table 1.

#### 4. FAILURE MODELS

In the domain of matrix dominated fracture, the controlling fracture propagating planes could occur at various different angles within a laminate. These angles depend on the ply orientations. This kind of behavior will be illustrated later in Section 6 and explained with more details. This type of failure mechanism lead us believe that the strength has to be predicted using a model based on ply-by-ply analysis. Any failure criterion developed on the laminate basis [5] may not be applicable. The reasons are: (1) there are more than one controlling fracture propagating planes and; (2) the lack of strength uniformity between plies along any direction. In other words, only a fraction of the laminate may fail along a direction while the others remain intact in the same plane. From the stress analysis of the  $[\pm 45_2]_S$  laminate, shown in Figure 2, one may think that the failure of a  $[\pm \phi]_S$  laminate will initiate on the axis normal to the applied load, which is based on the concept that failure will occur at the location of the maximum tangential stress. However, this idea will be shown incorrect in Section 6. In an earlier work [6], two models were proposed for the strength prediction of multidirectional composite laminates containing stress concentrations. The application of those models for the present study will be discussed in the following subsections.

#### 4.1 Point Strength Model (PSM)

The ultimate strength ratio of a notched composite laminate versus unnotched laminate is predicted using the first-ply-failure (FPF) strength of the notched laminate divided by the FPF strength of the corresponding unnotched laminate. The FPF strength of a notched laminate is calculated at the point with a characteristic length  $b_1$  along the assumed fracture propagating plane, Figure 3. In the case of matrix dominated failure, the fracture propagating planes occur along the fiber orientations. The notched strength reduction factor (SRF) can be written explicitly as

$$\text{SRF} = \frac{\sigma_N^\infty \quad \text{FPF notched strength at the point } (0, b_1)}{\sigma_0 \quad \text{FPF unnotched strength}} \quad (13)$$

where  $\sigma_N^\infty$  and  $\sigma_0$  denote the ultimate notched strength and the ultimate unnotched strength, respectively. The relations stated in Equations (13) and (15) are based on the assumption that the ratio of the FPF strength is the same as the ratio of the ultimate strength.

#### 4.2 Minimum Strength Model (MSM)

Once the laminate stresses are computed using Equations (1-6), the classical laminated plate theory is applied to calculate the ply stresses. Then an appropriate FPF criterion is utilized to compute the FPF strength at many selected points along the characteristic curve, denoted by the dotted line in Figure 1, which can be expressed as

$$\frac{x^2}{(a + b_0)} + \frac{y^2}{(b + b_0)} = 1 \quad (14)$$

where  $b_0$  (characteristic length) is a distance between the opening and the characteristic curve. In the case of circular openings, 90 points were analyzed for a range of  $0^\circ \leq \theta \leq 180^\circ$  along the characteristic curve, whereas in the case of sharp cracks, 180 points were analyzed for the same range of angle. The minimal FPF strength is obtained from the comparison of the solutions calculated at these points. This minimal FPF notched strength divided by the FPF strength of the corresponding unnotched laminate yields the strength reduction factor, which is proposed to be the same as the ultimate strength reduction factor:

$$\sigma_N^\infty \quad \text{Minimal FPF notched strength}$$

$$\text{SRF} = \frac{\sigma_0}{\text{FPF unnotched strength}} = \text{-----} \quad (15)$$

where the parameters have all been defined. This model can be applied to predict the SRF and the initiation locations of failure of a notched laminate.

Several FPF criteria are available in the literatures. The quadratic failure criterion (Tsai-Wu) with the stress interaction term  $F_{12}^* = -0.5$  was adopted in this analysis.

## 5. FINITE-WIDTH CORRECTION FACTORS

The finite-width correction factors (FWCF) of anisotropic or orthotropic laminates containing an elliptical opening have been derived in an earlier paper [8]. The accuracy of the analytical solution was assured by a finite element solution as well as experimental data. These correction factors were applied to interpolate the testing data.

Using the material properties listed in Table 1, the finite-width correction factors,  $K_T/K_T^\infty$ , for the AS4/3502  $[\pm\phi_2]_S$  family of laminates and an isotropic plate with a circular hole were plotted in Figure 4. The comparison shows that the FWCF for some of the  $[\pm\phi_2]_S$  family of laminates are higher than that of the isotropic plate, and some are lower. For instance, the FWCF of the  $[\pm30_2]_S$ ,  $[\pm45_2]_S$  and  $[\pm60_2]_S$  laminates at  $2a/W = 0.5$  are 1.355, 1.394 and 1.477, respectively, whereas the FWCF of an isotropic plate is 1.417 which is closest to that of the  $[\pm45_2]_S$  laminate. These FWCF are applied in such a way that they are multiplied by the testing data to obtain the infinite plate solution.

## 6. EXPERIMENT AND RESULTS

An experimental program was planned to study the matrix dominated mixed-mode fracture of notched and unnotched laminates under uniaxial tensile loading. The sensitivity of the notched strength of unidirectional composite laminates due to the discontinuity of holes and cracks was also investigated.

### 6.1 Procedures

The Hercules graphite/epoxy AS4/3502 preprag (tape form) was chosen to fabricate some  $[\pm\phi_2]_S$  laminates where  $\phi = 0^\circ, 30^\circ, 45^\circ$  and  $60^\circ$ . Five different sizes of holes and cracks were prepared. They are approximately 0.05, 0.1, 0.3, 0.4 and 0.6 inch. The circular holes in the laminates were produced using diamond impregnated drills. The central cracks were fabricated by first drilling a 0.01 inch diameter central hole and then completing the crack by a 0.005 inch diameter diamond coated wire. All the opening-to-width ratios of the specimens were arranged within 33 percent. After the specimens were

prepared, they were loaded in tension at a cross head speed of 10 or 20 lb/s. The material properties were characterized and given in Table 1.

## 6.2 Failure Mechanism

In the case of  $[0_8]$  laminates containing either a circular hole or a central crack, failure initiates with fiber-matrix splitting at the opening edges on the axis normal to the applied load. After the splitting occurs, the laminate is separated into load-carrying and non-load-carrying regions. The portions on the top and below of the opening are non-load-carrying regions. At this stage, this laminate becomes fully notch insensitive. This point is verified in Section 7 with the notched strength plotted versus opening-to-width ratio. Therefore, the controlling final fracture planes could occur in any place between the endtags at the load-carrying portions of the laminate.

All the fracture planes occur across the openings for the  $[\pm\phi_2]_S$  laminates studied in this paper. Some samples of the failed specimens containing circular holes are illustrated in Figure 5. The fracture planes all took place along the  $+\phi$  and  $-\phi$  fiber directions. The failure initiation locations, however, are somewhat different for different hole sizes. When the hole size is small, the opening has very little influence on the laminate strength, and the failure initiation locations,  $\theta$ , coincide with the ply-angles, i.e.  $\theta = \pm 30^\circ, \pm 45^\circ$  and  $\pm 60^\circ$  for the  $[\pm 30_2]_S, [\pm 45_2]_S$  and  $[\pm 60_2]_S$  laminates, respectively. When the hole size is large, the fracture propagating planes were found tangent or nearly tangent to the opening. The angles measured from the loading axis were  $\pm 60^\circ$  for the  $[\pm 30_2]_S$  laminates,  $\theta = \pm 46^\circ \sim \pm 60^\circ$  for the  $[\pm 45_2]_S$  laminates and  $\theta = \pm 38^\circ \sim \pm 70^\circ$  for the  $[\pm 60_2]_S$  laminates.

The failed patterns of the  $[\pm\phi_2]_S$  laminates containing a normal crack under tensile loading are shown in Figure 6. In this case, all the failures initiate from the crack tips and propagates along the fiber direction, i.e.  $\theta = \phi^\circ$ . For instance, the failure initiation locations are  $\theta = \pm 30^\circ$  for the  $[\pm 30_2]_S$  laminate.

## 6.3 Notched Strength

The gross strength,  $\sigma_N$ , of a laminate was calculated by the fracture load divided by the total cross sectional area of the specimen. The finite width correction factors, Figure 4, were then applied to obtain the notched strength,  $\sigma_N^\infty$ , of the infinite plate. The results of the  $[0_8]$  laminates containing either a circular hole or a normal crack are listed in Table 2. Tables 3 and 4 contain the configuration and ultimate strength of the  $[\pm 30_2]_S, [\pm 45_2]_S$  and  $[\pm 60_2]_S$  laminates containing a circular hole and a crack, respectively.

## 7. CORRELATION OF THEORY WITH EXPERIMENT

The experimental data was utilized to examine the predictions for the notched strength using the PSM and the MSM, as well as the predicted failure initiation locations using the MSM. The characteristic lengths,  $b_1$  and  $b_0$ , were considered as two constants first, then as a power function of the opening size.

### 7.1 Characteristic Length As a Constant

The characteristic lengths,  $b_1$  and  $b_0$ , were determined by the back substitution of one notched strength data into Equations (1-10) and the strength models, Equations (13) or (15). The comparisons of the prediction using the MSM and the experimental data are illustrated in Figure 7 for the uniaxial  $[0]_8$  laminate and the  $[\pm 30]_2$ <sub>S</sub>,  $[\pm 45]_2$ <sub>S</sub> and  $[\pm 60]_2$ <sub>S</sub> laminates with circular openings. In these figures, the line of net strength (notch insensitive line) represents the fracture load divided by the net cross-sectional area. The result shows that the gross strength of the  $[0]_8$  laminate, Figure 7a, scatter closely to the line of net strength, which means that the ultimate notched strength is fully notch insensitive. The predicted notched strength for the other laminates generally agrees reasonably well with the experimental data. The predicted initiation locations of failure for the  $[\pm 30]_2$ <sub>S</sub> laminate are from  $\theta = \pm 27^\circ$  to  $\pm 59^\circ$  for small hole to large hole, respectively. These predictions are almost identical with the experimental observation, which are  $\pm 30^\circ$  and  $\pm 60^\circ$  for small hole and large hole, respectively. When the hole is small, the predicted failure initiation locations of the  $[\pm 45]_2$ <sub>S</sub> and  $[\pm 60]_2$ <sub>S</sub> laminates are at  $\theta = \pm 49^\circ$  and  $\pm 60^\circ$ , respectively, whereas the experimental results were at  $\theta = \pm 45^\circ$  and  $\pm 60^\circ$ , respectively. When the hole radius is larger than 0.2 inches, the predicted failure initiation locations are at  $\theta = 90^\circ$ , which is less accurate than the prediction for the case with a small hole. This is also the point that the prediction changes the slope of its curve, Figures 7c-d, and deviates from the data. It is interesting to note that the characteristic lengths  $b_0$  for the  $[\pm 30]_2$ <sub>S</sub> and  $[\pm 60]_2$ <sub>S</sub> laminates (both are 0.12 inch) are symmetric with respect to that of the  $[\pm 45]_2$ <sub>S</sub> laminate ( $b_0 = 0.08$  inch).

Using the anisotropic finite width correction factor in Section 5, the predicted notched strength (infinite width plate) can be converted into finite-width gross strength. The result is plotted as a function of the opening-to-width ratio in Figure 8a. For convenience the width of the plate has been chosen as unity. The gross strength of the present  $[\pm \phi]_2$ <sub>S</sub> laminates lie beneath the line of net strength. This characteristic reveals that these laminates are notch sensitive. The gross strength of these laminates were obtained by multiplying the gross strength reduction factor by the unnotched strength,  $\sigma_0$ , Figure 8b.

The predictions of the  $[\pm\phi_2]_S$  family of laminates containing a central normal crack are compared to the experimental results in Figure 9. The strength of the unidirectional  $[0_8]$  laminate with a central crack is shown notch insensitive. For the  $[\pm\phi_2]_S$  laminates containing a crack, the locations of the initiation of failure,  $\theta$ , can be visualized as the same to the ply orientations (i.e.,  $\theta = \pm\phi^\circ$ ). Thus, the prediction of the PSM was also examined by the experimental data.

It is a surprise to see that the notched strength of the  $[\pm 30_2]_S$  laminate increases for crack length ( $2a$ ) larger than 0.12 inch. The application of the MSM does not correlate very well with the data in this case. When the PSM was applied, the characteristic length,  $b_1$ , was measured along the fiber direction at an angle  $\theta = \phi^\circ$  from the crack tips. The prediction does agree with the trend of the unexpected experimental result. In the case of  $[\pm 45_2]_S$  laminate, the prediction using the PSM agrees very well with the experimental data. Utilizing the MSM, the predicted failure initiation locations were at  $\theta = \pm 50^\circ \sim \pm 56^\circ$  (small to large hole) and  $\theta = 52^\circ \sim 58^\circ$  for the  $[\pm 45_2]_S$  and  $[\pm 60_2]_S$  laminates, respectively. These results are acceptable as compared to the experimental observation, which are  $\pm 45^\circ$  and  $\pm 60^\circ$ , respectively.

## 7.2 Characteristic Length As a Power Function

In the case of fiber dominated composite laminates containing elliptical openings, the characteristic length  $b_o$  can be expressed in a simple form [9]. A laminate with an implanted crack has been simulated very well by an elliptical opening with the aspect ratio  $a/b = 50$ . The characteristic length  $b_o$  for a laminate with a crack was found double in magnitude compared to the one with a circular opening. Earlier investigation has shown that excellent agreement between predicted notched strength and data was achieved if the characteristic length  $b_o$  is expressed as a function of the hole size. Following the same approach for the fiber dominated laminates, the characteristic length for matrix dominated laminates can be written as

$$b_o = m_o (a/a_r)^n (a/b)^{0.177} \quad (16)$$

where  $m_o$  and  $n$  are constants to be determined by the back substitution of two or more data points of notched strength into the failure model, and  $a_r$  is a reference radius introduced to make the quotient in the parenthesis nondimensional.

When Equation (16) was utilized, the predicted notched strength for the AS4/3502  $[\pm 45_2]_S$  and  $[\pm 60_2]_S$  laminates with holes and cracks were compared to experimental data in Figures 10 and 11, respectively. The correlation between theory and data was reasonably well. Using the  $b_o$  shown in Figures 10 and 11, the predicted gross strength reduction factor as a function of the opening-to-width ratio for these laminates with central

cracks are illustrated in Figure 12a. Figure 12b illustrates the magnitude of the predicted gross strength. The deviation of these curves from the line of net strength shows that these laminates are notch sensitive. It is of interest to see that the gross strength of the  $[\pm 60_2]_S$  laminate is slightly higher than the line of net strength. The gross strength of the  $[\pm 45_2]_S$  laminate intersects with the line of net strength at about  $2a/w = 0.45$ . This laminate layup also has a trend of having higher strength than the line of net strength for  $2a/w > 0.45$ .

## 8. DISCUSSIONS AND CONCLUSION

The mixed-mode fracture of matrix dominated composite laminates containing stress concentrations was studied using the AS4/3502  $[\pm\phi_2]_S$  family of laminates with central holes and normal cracks. In the case of circular holes, all the gross strength of the laminates considered here are lower than the line of net strength except the  $[0_8]$  laminates, which scatter closely along the line of net strength. In the case of central normal cracks, some interesting results were observed:

(1) The notched strength of the  $[\pm 30_2]_S$  laminate, Figure 9, increases for crack length,  $2a$ , larger than 0.12 inch.

(2) The gross strength of the  $[\pm 30_2]_S$  and  $[\pm 60_2]_S$  laminates containing central cracks are higher than the line of net strength, Figures 9 and 12. This surprising result, however, agrees with the prediction using the PSM.

Fiber-matrix splitting was observed for unidirectional  $[0_8]$  laminates at the edges of the holes and at the crack tips. After the splitting process extends to a large proportion of the laminate, the laminate separates into load-carrying and non-load-carrying regions. Regardless the shape of the opening, the total volume of the load-carrying sections are the same for a laminate with a given opening length,  $2a$ . This is why the ultimate strength of a  $0^\circ$  laminate is notch insensitive.

If the performance of a laminate is affected by the stress concentrations, it is "notch sensitive". For example, a  $[\pm 30_2]_S$  laminate is notch sensitive because its ultimate strength scatters away from the line of net strength. If the performance of a notch laminate is affected by the change of opening shape with a same opening length ( $2a$ ), the laminate is defined as "notched shape sensitive". We conclude from this study that a  $[0_8]$  laminate is notch insensitive and notched shape insensitive, Figures 7a and 9a. The notched strength of the  $[\pm 45_2]_S$  laminate is notched shape insensitive, Figure 10, although it is notch sensitive, as shown in Figures 8 and 12. The notched strength of the  $[\pm 60_2]_S$  laminate is notched shape sensitive, Figure 11, and notch sensitive, Figures 8 and 12.

From this result, a reasonable thought arises that any multidirectional graphite/epoxy laminate containing a major proportion of  $0^\circ$  and  $\pm 45^\circ$  laminae is likely to be notched shape insensitive. This idea agrees with the data presented in References 3, 10 and 11 using  $[\pm 45/0_2]_S$ ,  $[0/90/\pm 45]_S$  and  $[0/90/\pm 45]_{2S}$  laminates, respectively. We also conclude from this study that most laminates are notched shape sensitive. Although a unidirectional  $0^\circ$  laminate is notch insensitive, it can become notch sensitive and notched shape sensitive in the presence of constraint plies, such as  $[0/90_2/0]_S$  laminate [10]. In the second part of this work, very good agreement between theory and experimental data has been obtained for the mixed-mode fracture of matrix dominated composite laminates under compressive loading, which will be published elsewhere.

### ACKNOWLEDGEMENT

The author wish to acknowledge Dr. S. W. Tsai of the Materials Laboratory, Wright Patterson Air Force Base, for his support of this work.

### REFERENCES

1. Morris, D. H. and H.T. Hahn, "Mixed-Mode Fracture of Graphite/Epoxy Composites: Fracture Strength," J. of Composite Materials, 2:124-138 (1977).
2. Tan, S. C., "Mixed-Mode Fracture of Notched Composite Laminates Under Uniaxial and Multiaxial Loading," Engineering Fracture Mechanics, 31:733-746 (Dec. 1988).
3. Mar, J. W. and K. Y. Lin, "Fracture of Boron/Aluminum Composites with Discontinuities," J. of Composite Materials, 11:405-421 (Oct. 1977).
4. Chang, F. K and K. Y. Chang, "A Progressive Damage Model for Laminated Composites Containing Stress Concentrations," J. of Composite Materials, 21:834-855 (1987).
5. Awerbuch, J and Madhukar, M. S., "Notched Strength of Composite Laminates: Predictions and Experiments - A Review," J. of Reinforced Plastics and Composites, vol. 4 (Jan. 1985).
6. Tan, S. C., "Notched Strength Prediction and Design of Laminated Composites Under In-Plane Loadings," J. of Composite Materials, 21:750-780 (August 1987).
7. Lekhnitskii, S. G., Anisotropic Plates, translated from the second Russian edition by Tsai, S. W. and T. Cheron, Gordon and Breach (1968).
8. Tan, S. C, "Finite-Width Correction Factors for Anisotropic Plate Containing A Central Opening," J. of Composite Materials, 22:1080-1097 (November 1988).
9. Tan, S. C., "Effective Stress Fracture Models for Unnotched and Notched Multidirectional Laminates," J. of Composite Materials, 22:322-340 (April 1988).

10. Tan, S. C., "Fracture Strength of Composite Laminates With an Elliptical Opening," *Composite Science and Technology*, 29:133-152 (1987).

11. Backlund, J. and Aronsson C. G., "Tensile Fracture of Laminates With Holes," *J. of Composite Materials*, 20:259-286 (1986).

## FIGURE CAPTIONS

Figure 1. Coordinates system of an infinite composite laminate containing an opening. Dotted line is the characteristic curve.

Figure 2. Tangential stress distribution,  $\sigma_\theta$ , at various characteristic curves of a graphite/epoxy  $[\pm 45_2]_S$  laminate with a circular hole.

Figure 3. The characteristic length  $b_1$ , used for the Point Strength Model, is measured along the assumed fracture propagating plane.

Figure 4. Finite-width correction factors for AS4/3502  $[\pm \phi_2]_S$  laminates and isotropic plate with a central hole.

Figure 5. Failed patterns of the Gr/Ep AS4/3502  $[\pm 30_2]_S$  (left) and  $[\pm 60_2]_S$  (right) laminates with a circular hole.

Figure 6. Failed patterns of the Gr/Ep  $[\pm 30_2]_S$  (left) and  $[\pm 60_2]_S$  (right) containing a central crack.

Figure 7. Comparison of the predicted notched strength (MSM) and the experimental data for the  $[\pm \phi_2]_S$  laminates with a central hole.

Figure 8. Gross strength reduction factor and magnitude versus opening-to-width ratio for the  $[\pm \phi_2]_S$  laminates with a central hole.

Figure 9. Correlation of the predicted strength (PSM and MSM) and the experimental data for the  $[\pm \phi_2]_S$  laminates containing a central crack.

Figure 10. Experimental data and predicted notched strength using a modified  $b_o$  (MSM) for the  $[\pm 45_2]_S$  laminate.

Figure 11. Experimental data and predicted notched strength using a modified  $b_o$  for the  $[\pm 60_2]_S$  laminate.

Figure 12. Predicted gross strength reduction factor and magnitude as a function of the opening-to-width ratio for the  $[\pm \phi_2]_S$  laminates with a central crack.

Table 1a. Elastic properties of the graphite/epoxy AS4/3502 lamina.

Parameters	GPa	(10 <sup>6</sup> psi)
Longitudinal modulus, E <sub>11</sub>	143.92	(20.87)
Transverse modulus, E <sub>22</sub>	11.86	( 1.72)
In-plane shear modulus, G <sub>12</sub>	6.69	( 0.97)
Poisson's ratio, ν <sub>12</sub>	0.3257	

Table 1b. Strength properties.

Parameters	MPa	(Ksi)
Longitudinal tensile strength, X	1861.6	(270)
Longitudinal compressive strength, X'	1482.4	(215)
Transverse tensile strength, Y	51.7	(7.5)
Transverse compressive strength, Y'	206.8	(30)
In-plane shear strength, S	65.0	(9.4)

Table 2. Experimental results\* for the graphite/epoxy AS4/3502 [0<sub>8</sub>] laminate containing a circular hole or a central crack.

Opening shape	Opening length 2a (mm)	Plate width (mm)	Gross strength σ <sub>N</sub> (MPa)	σ <sub>N</sub> σ <sub>o</sub>	Variation (%)
Circular	0	24.97	1861.6	1.000	
Circular	1.17	12.37	1627.2	0.872	± 0.9
Circular	2.52	12.37	1461.7	0.784	± 1.3
Circular	7.52	24.97	1434.1	0.769	± 0.7
Circular	10.31	31.80	1399.6	0.752	± 5.6
Circular	15.42	46.23	1234.2	0.661	± 8.3
Crack	0	24.99	1861.6	1.000	
Crack	1.22	12.32	1496.2	0.803	± 5.0
Crack	2.82	12.32	1323.8	0.709	
Crack	7.49	24.97	1282.4	0.689	± 0.0
Crack	9.91	31.80	1068.7	0.572	± 0.4
Crack	15.52	46.23	1220.4	0.653	

\* Average of two specimens.

Table 3. Experimental results\* for the Gr/Ep AS4/3502:(a)  $[\pm 30_2]_s$ , (b)  $[\pm 45_2]_s$ , (c)  $[\pm 60_2]_s$  laminates with a circular hole.

Layup	Hole diameter 2a (mm)	Plate width (mm)	Gross strength $\sigma_N$ (MPa)	Notched strength $\sigma_{N^\infty}$ (MPa)	$\sigma_{N^\infty}$ $\sigma_0$	Variation (%)
(a)	0	24.97	--	392.3	1.000	$\pm 0.8$
(a)	1.17	12.34	308.9	364.9	0.929	$\pm 1.8$
(a)	2.52	12.37	280.6	343.4	0.875	$\pm 0.5$
(a)	7.62	24.97	206.3	268.1	0.683	$\pm 1.3$
(a)	10.34	31.80	229.6	258.8	0.659	$\pm 4.9$
(a)	15.47	46.20	244.8	277.8	0.708	$\pm 0.8$
(b)	0	24.97	--	130.3	1.000	$\pm 3.7$
(b)	1.17	12.37	120.7	121.4	0.934	$\pm 2.2$
(b)	5.18	12.37	97.9	102.2	0.786	$\pm 1.9$
(b)	7.65	24.99	84.1	93.3	0.717	$\pm 6.2$
(b)	10.36	31.80	76.5	86.5	0.666	$\pm 2.0$
(b)	15.44	46.23	78.6	89.4	0.687	$\pm 2.9$
(c)	0	24.97	--	51.3	1.000	$\pm 0.8$
(c)	1.17	12.34	50.9	51.4	1.003	$\pm 1.6$
(c)	2.52	12.34	43.9	45.9	0.897	$\pm 4.7$
(c)	7.59	24.99	36.8	41.2	0.803	$\pm 1.9$
(c)	10.36	31.80	33.1	37.7	0.736	$\pm 6.6$
(c)	15.52	46.25	33.7	38.8	0.756	$\pm 4.2$

\* Average of two specimens.

Table 4. Experimental results\* for the Gr/Ep AS4/3502:(a)  $[\pm 30_2]_s$ , (b)  $[\pm 45_2]_s$ , (c)  $[\pm 60_2]_s$  laminates with a center crack.

Layup	Crack length 2a (mm)	Plate width (mm)	Gross strength $\sigma_N$ (MPa)	Notched strength $\sigma_{N^\infty}$ (MPa)	$\sigma_{N^\infty}$ $\sigma_0$	Variation (%)
(a)	0	24.99	--	392.3	1.000	$\pm 0.8$
(a)	1.29	12.32	348.2	349.6	0.890	$\pm 2.4$
(a)	2.59	12.32	324.7	327.5	0.834	$\pm 6.4$
(a)	7.62	24.99	326.1	339.9	0.872	$\pm 2.5$
(a)	10.14	31.83	332.3	347.5	0.892	$\pm 0.2$
(a)	15.14	46.23	350.9	368.2	0.945	$\pm 2.4$
(b)	0	24.99	--	130.3	1.000	$\pm 3.7$
(b)	1.47	12.32	116.5	116.5	0.900	$\pm 4.5$
(b)	2.74	12.32	99.3	101.4	0.777	$\pm 0.4$
(b)	7.54	24.99	92.4	95.8	0.742	$\pm 3.2$
(b)	10.06	31.80	87.6	91.0	0.702	$\pm 2.6$
(b)	15.16	46.25	88.9	93.8	0.719	$\pm 1.3$
(c)	0	24.99	--	51.3	1.000	$\pm 0.7$
(c)	1.35	12.32	52.9	53.2	1.038	$\pm 1.6$
(c)	2.67	12.32	47.7	48.6	0.949	$\pm 0.2$
(c)	7.47	24.99	42.3	43.9	0.858	$\pm 3.3$
(c)	10.03	31.80	39.4	41.2	0.804	$\pm 4.7$
(c)	15.16	46.25	41.3	43.4	0.846	$\pm 3.9$

\* Average of two specimens.

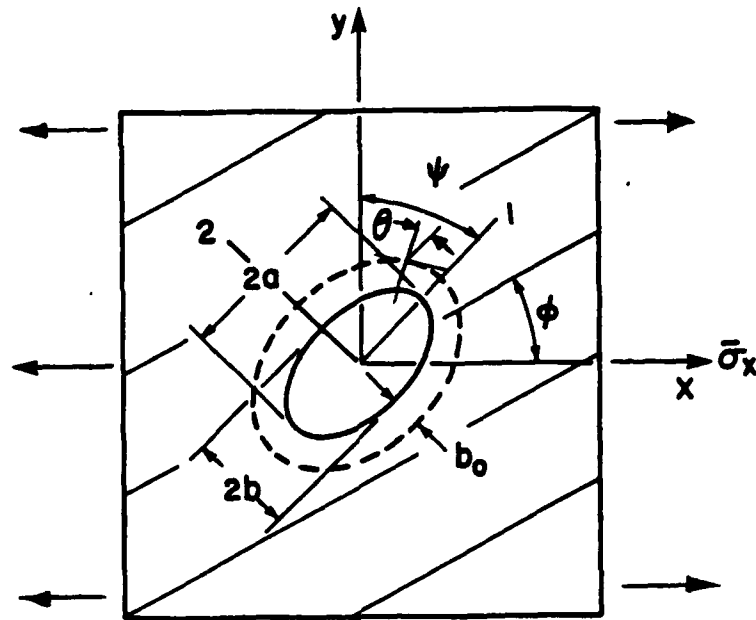


Figure 1. Coordinates system of an infinite composite laminate containing an opening. Dotted line is the characteristic curve.

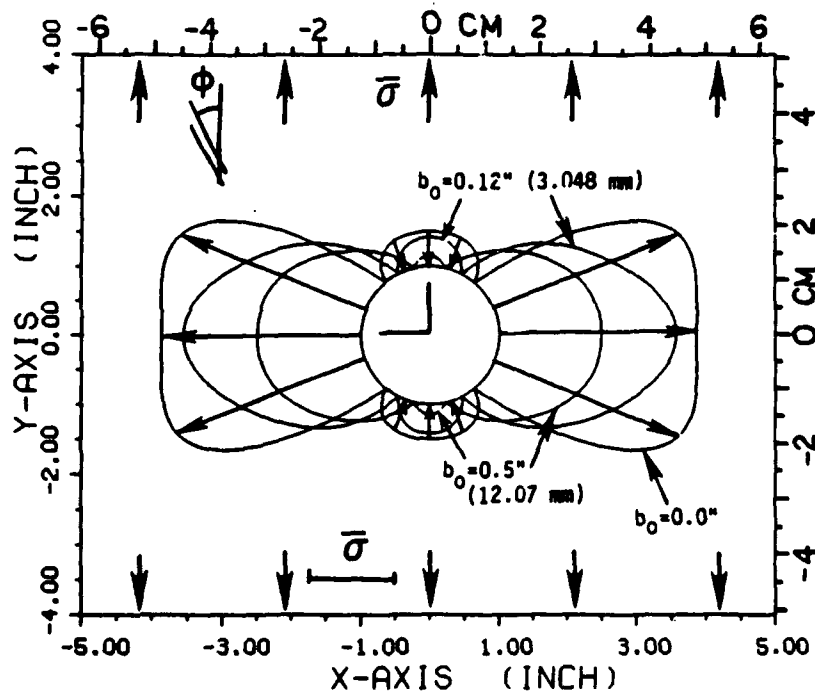


Figure 2. Tangential stress distribution,  $\sigma_\theta$ , at various characteristic curves of a graphite/epoxy  $[\pm 45_2]_s$  laminate with a circular hole.

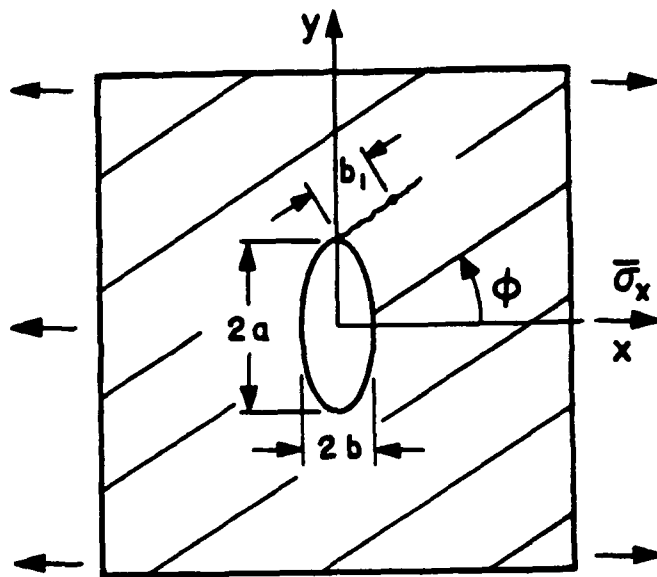


Figure 3. The characteristic length  $b_1$ , used for the Point Strength Model, is measured along the assumed fracture propagating plane.

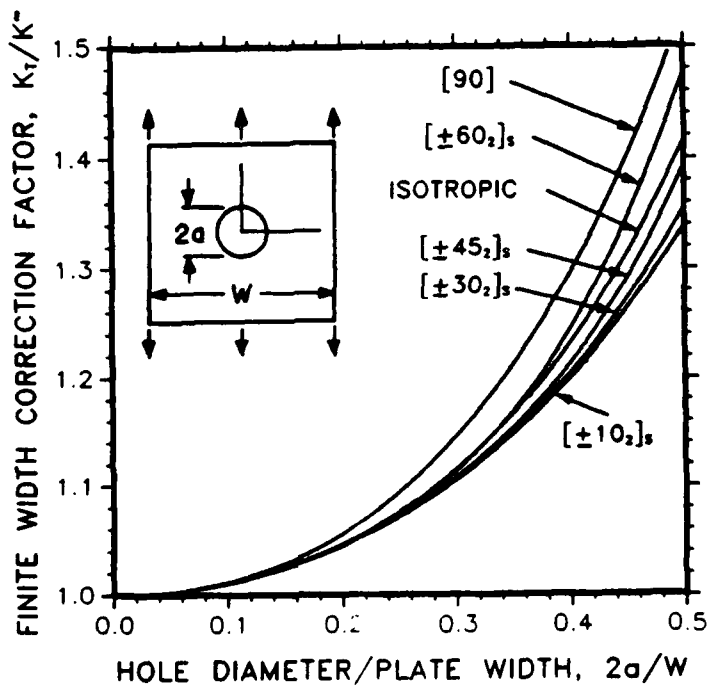


Figure 4. Finite-width correction factors for AS4/3502  $[\pm\theta_2]_s$  laminates and isotropic plate with a central hole.



Figure 5. Failed patterns of the Gr/Ep AS4/3502  $[\pm 30_2]_S$  (left) and  $[\pm 60_2]_S$  (right) laminates with a circular hole.



Figure 6. Failed patterns of the Gr/Ep  $[\pm 30_2]_S$  (left) and  $[\pm 60_2]_S$  (right) containing a central crack.

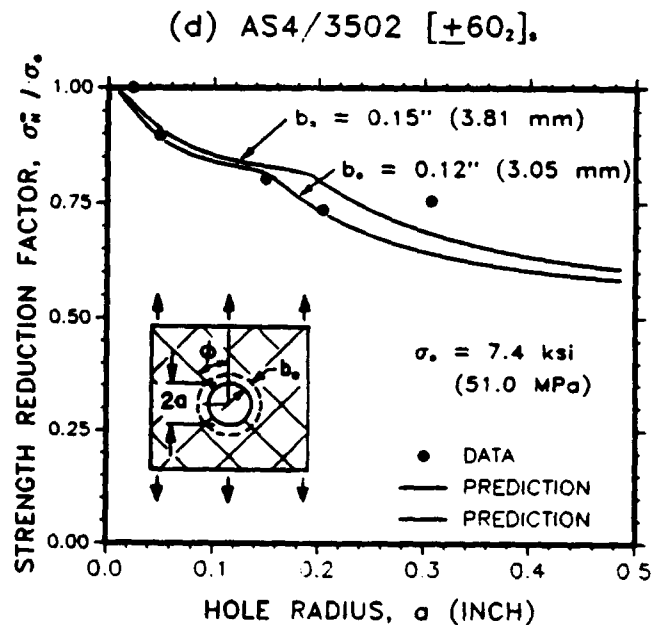
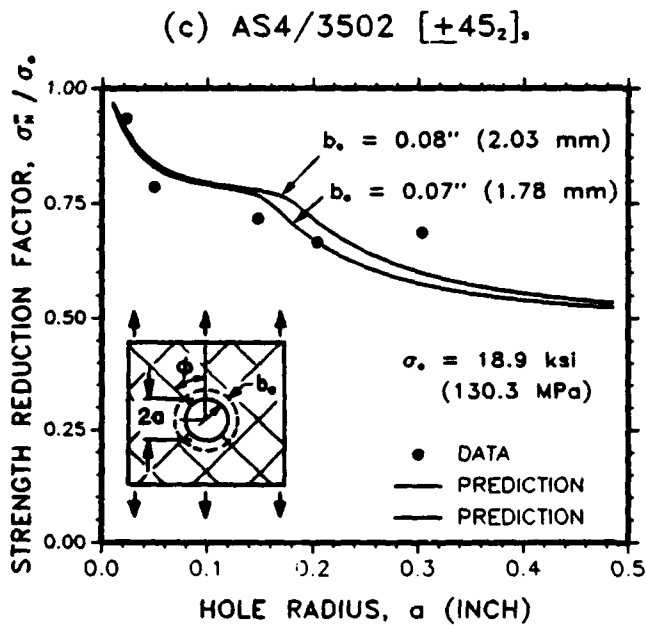
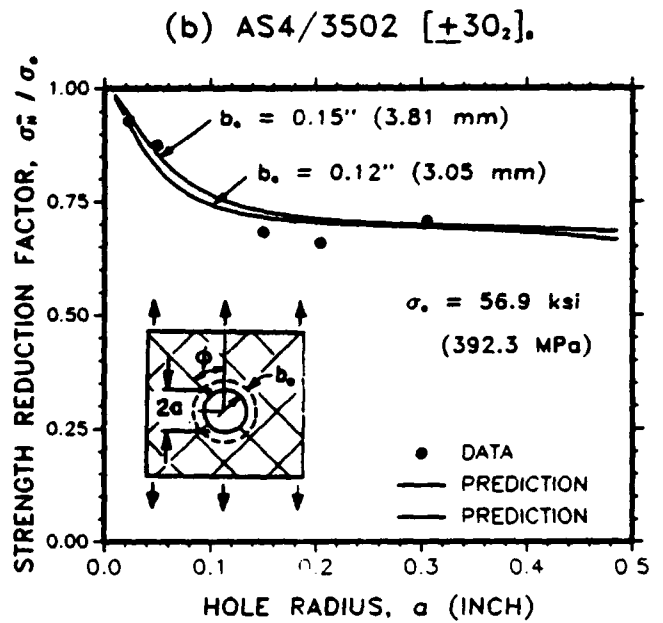
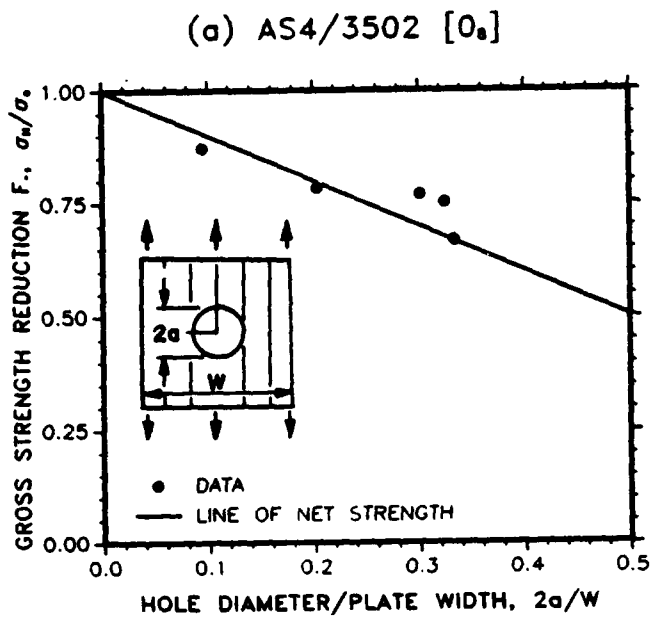
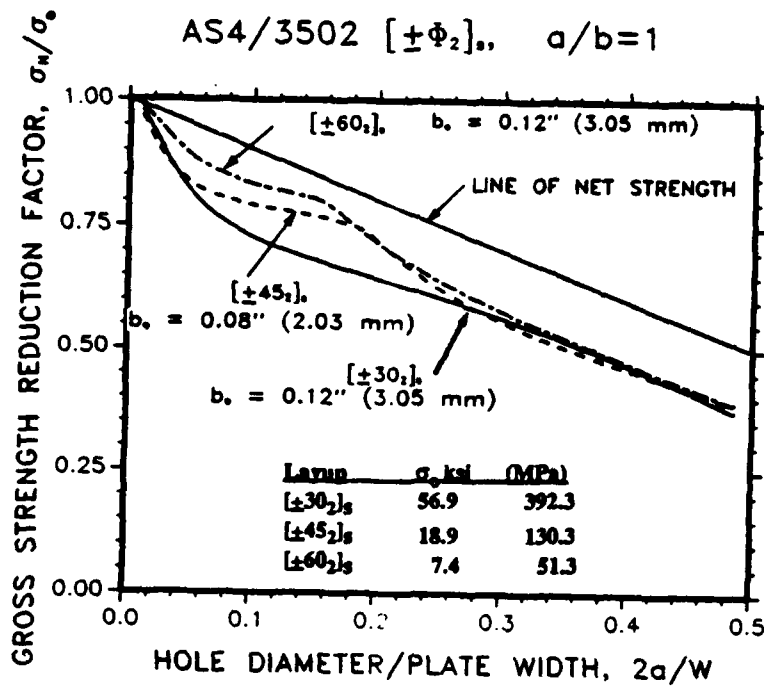
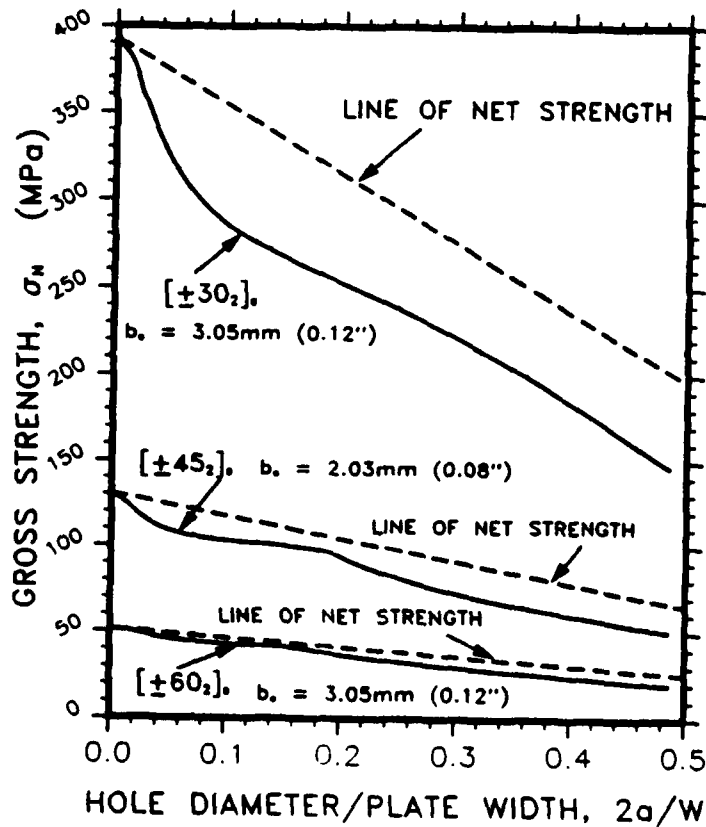


Figure 7. Comparison of the predicted notched strength (MSM) and the experimental data for the  $[\pm\phi_2]_s$  laminates with a central hole.



(a) Gross strength reduction factor



(b) Gross strength

Figure 8. Gross strength reduction factor and magnitude versus opening-to-width ratio for the  $[\pm\Phi_2]_s$  laminates with a central hole.

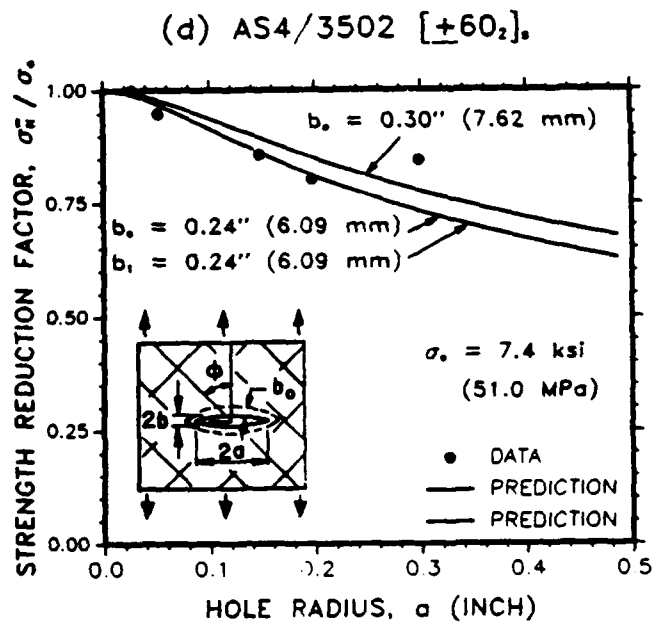
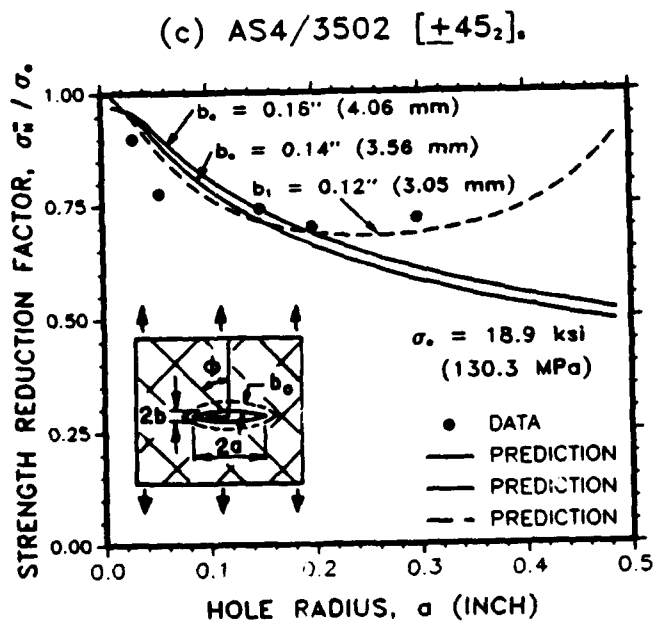
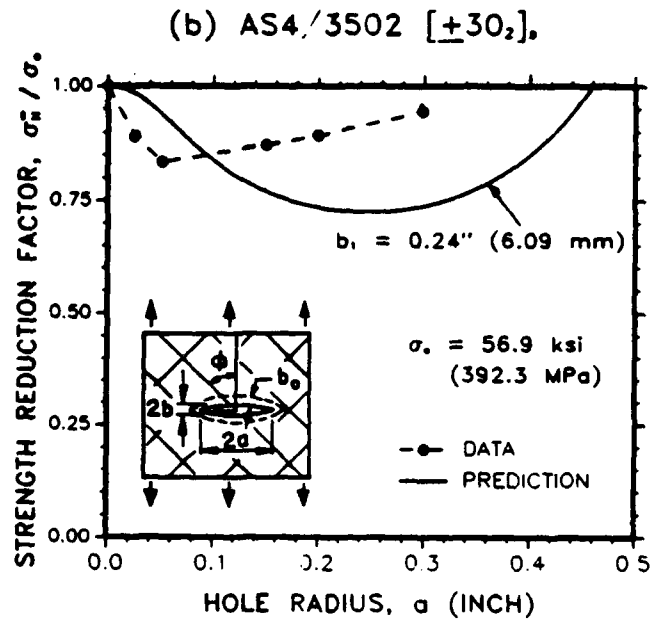
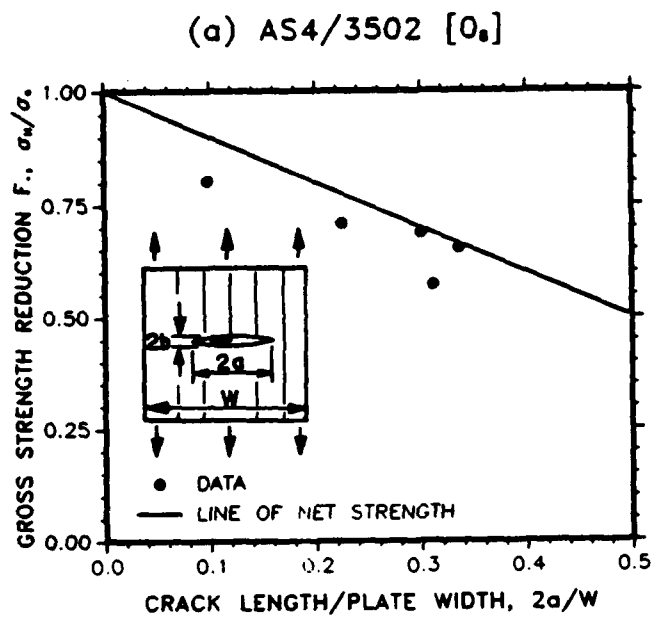


Figure 9. Correlation of the predicted strength (PSM and MSM) and the experimental data for the  $[\pm\theta_2]_s$  laminates containing a central crack.

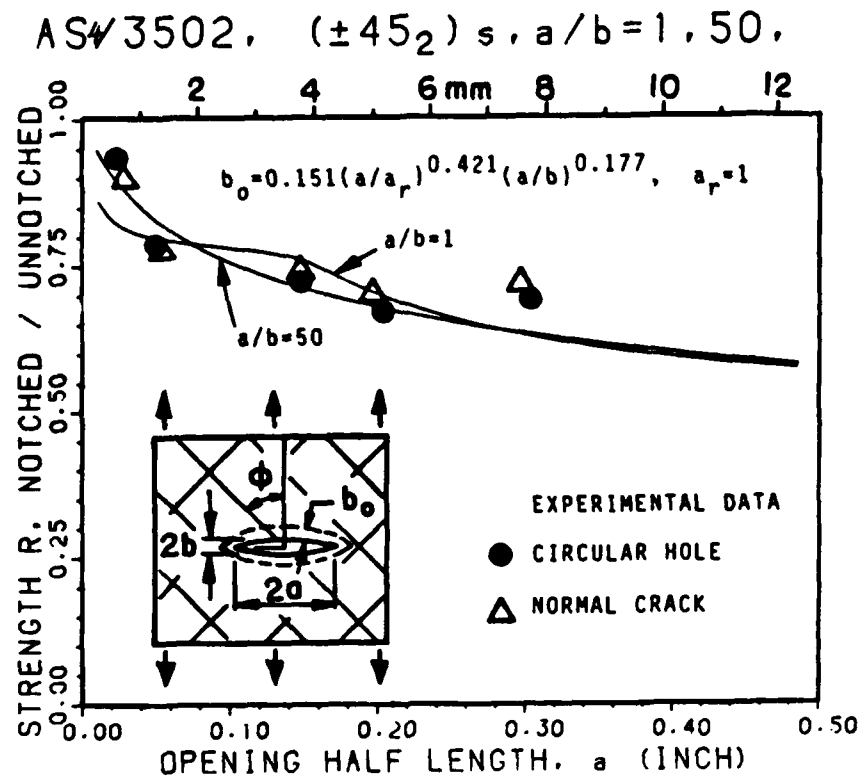


Figure 10. Experimental data and predicted notched strength using a modified  $b_0$  (MSM) for the  $[\pm 45_2]_s$  laminate.

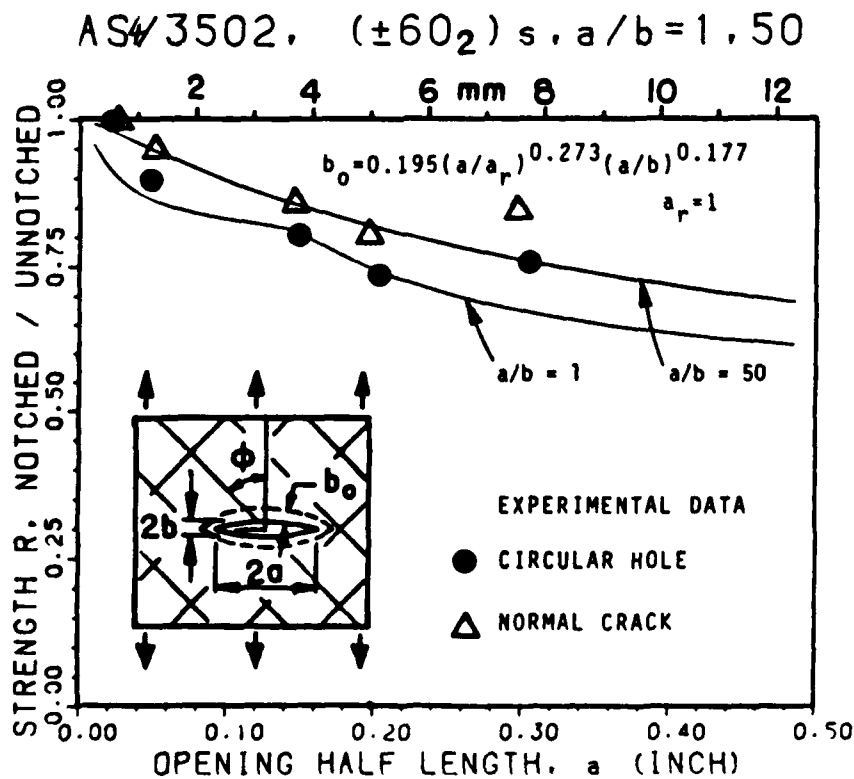
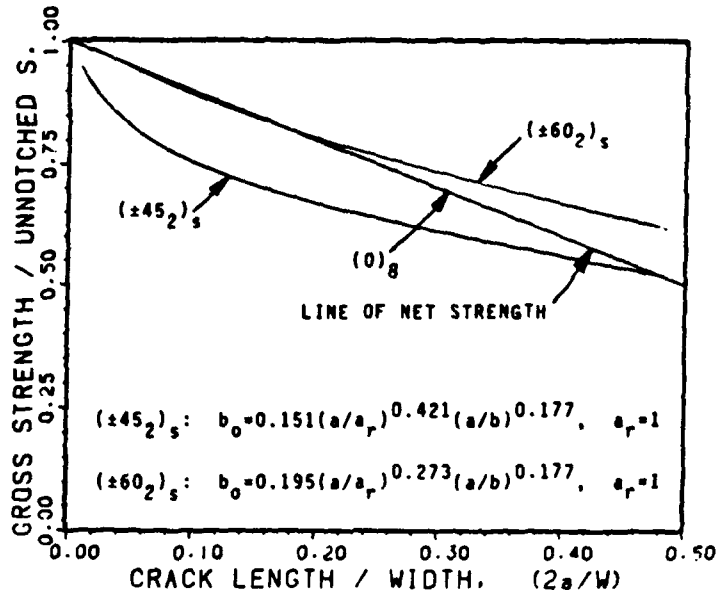
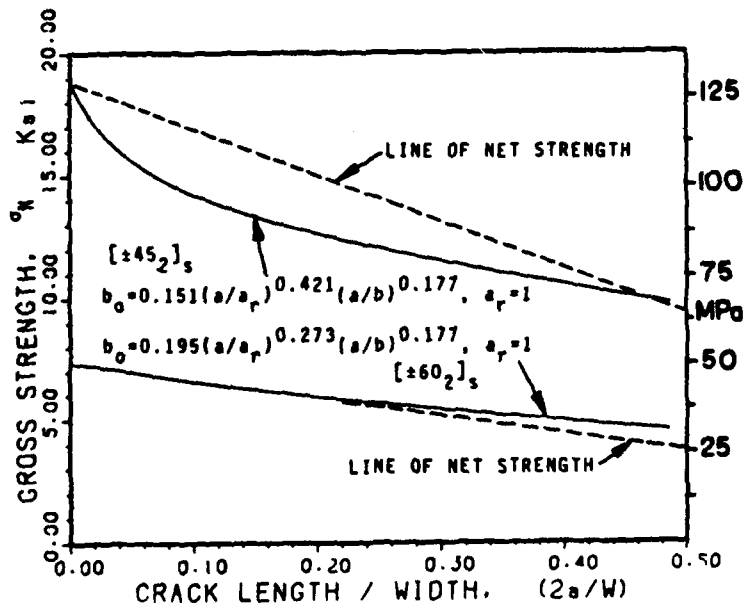


Figure 11. Experimental data and predicted notched strength using a modified  $b_0$  for the  $[\pm 60_2]_s$  laminate.

ASW3502,  $(\pm\phi_2)_s$ ,  $a/b=50$



(a) Gross strength reduction factor



(b) Gross strength

Figure 12. Predicted gross strength reduction factor and magnitude as a function of the opening-to-width ratio for the  $[\pm\phi_2]_s$  laminates with a central crack.

## **SECTION II**

# **THERMO-ELASTIC MODEL FOR MULTIDIRECTIONAL COATED FIBER COMPOSITES: TRACTION FORMULATION**

## ABSTRACT

In this work a companion model to that given earlier is developed to approximate the thermoelastic response of a composite body reinforced by coated fibers oriented in various directions. The fundamental representative volume element is a three-phase concentric circular cylinder under prescribed surface tractions which are independent of the axial coordinate. The analysis leads to a lower bound calculation of the effective moduli, which together with the upper bound results, provides a more precise estimate of the overall composite properties. A parametric study has been further conducted to illustrate the effect of different coating materials and thicknesses on the effective properties and micro-stress distribution within the constituents of a three-dimensional fibrous composite subjected to a uniform temperature change.

## 1. INTRODUCTION

Fiber reinforced composites have been widely used as structural components owing to their high specific stiffness and strength. In most of the applications, the fibers are uncoated. Recently, however, there has been a growing demand for coated fibers as a reinforcement in some new application areas such as electrical composites, metal matrix composites (MMC) and ceramic matrix composites (CMC) intended for high temperature applications.

In electrical composites, nonconductive fibers are coated with conductive metals to obtain the desired level of conductivity of the composite at reduced material cost. In MMC and CMC, the fiber coating can serve as diffusion barriers for fiber-matrix combinations that otherwise may be incompatible due to excessive reactions leading to fiber degradation. The coating can also act as a protective barrier for the fiber and prevent it from oxidation, thus enabling it to be used for extended periods of time in oxidizing environment. Coatings of different materials and of varying amounts have also been applied to the fiber to prevent or control the degree of bonding at the fiber-matrix interface leading to substantial improvements in the strength and damage tolerance of the composites [1-3]. The use of coatings as bonding control layers has also been successfully demonstrated for Boron/Epoxy [4], HT-S Carbon/Epoxy [5] and GY-70 Graphite/Epoxy [6] composites. For theoretical analysis, the interphase region between the fiber and the matrix can also be modeled as a coating layer [7]. Quite often, the interphase region is a product of the processing conditions involved in the manufacture of the composite.

A coated continuous fiber composite has been modeled by four concentric cylinders consisting of fiber, coating, matrix and surrounding composite body by Mikata and Taya [8]. All the thermoelastic properties of the surrounding body (composite) were determined by the use of rule of mixtures. The solution for the stress distribution for this unidirectionally aligned fiber composite was determined with the composite subjected to three independent axisymmetric boundary

conditions, namely, uniform temperature change, uniaxial applied stress and equal biaxial applied stress. An analytical model for composites reinforced in three orthogonal directions (3-D) and containing regions with degraded stress transfer characteristics across the fiber-matrix interface was developed by Chatterjee and Kibler [9]. In the DCAP model [9], upper and lower bounds on the effective elastic moduli and thermal expansion coefficients are obtained by assuming suitable displacement and stress fields and minimizing the potential and complementary energy, respectively.

The problem of a multidirectional coated fiber composite was recently treated by Pagano and Tandon [10]. The fundamental representative volume element was a three-phase concentric circular cylinder under prescribed displacement components. By use of the theory of elasticity, effective thermoelastic properties of the composite were determined and the microstress distribution within the constituents evaluated with the composite subjected to externally applied uniform mechanical and/or hygrothermal loading. This study reported results based on the displacement boundary conditions on the representative volume element which lead to an upper bound of the elastic stiffnesses.

In this paper, we will consider traction boundary conditions on the surface of the representative volume element. This approach will lead to a lower bound estimate of the composite effective moduli and together with the upper bound result will provide the bounding solutions for the composite properties. The composite cylinder assemblage model is, of course, a geometric idealization of a real fiber reinforced material. The experimental measurement of composite moduli should lie within the spread of the bounds and the tightness of the bounds will provide a measure of the accuracy of the analysis and the assumed geometric model.

The general solution for the stress and displacement field in a three-phase circular cylinder, under surface tractions which do not vary along the generator, will be presented first. Upper and lower

bound estimates of the effective thermoelastic properties of a unidirectional and a three-dimensional isotropic composite will be discussed next. Graphite/Epoxy and Nicalon/BMAS are the two material systems which we have chosen for the analysis. Finally, parametric study will be conducted to examine the influence of coating properties on the effective moduli and stress distribution within the constituents for the composite subjected to a uniform temperature change.

## 2. THE COMPOSITE MODEL

The composite model used in the analysis is similar to the one used by the authors in the displacement formulation [10] wherein a coated, continuous fiber reinforced composite is modeled by a representative volume element composed of  $N$  concentric circular cylinder elements, as shown in Figure 1. The fiber (innermost cylinder), coating and the matrix (outermost cylinder) are denoted by the indices  $p = 1, 2,$  and  $3,$  and their outer radii by  $r_1, r_2,$  and  $r_3,$  respectively. The composite volume between the elements is further denoted as the interstitial matrix region. The matrix in the composite cylinder as well as in the interstitial region could, in turn, be reinforced by particles.

Each element orientation,  $j,$  is defined via the two cylindrical angles  $\Omega$  and  $\Phi$  with respect to a fixed  $x_1 - x_2 - x_3$  coordinate system. The local element cartesian coordinate system is represented by  $X_1 - X_2 - X_3.$  It should be noted that the local fiber axis,  $X_1,$  coincides with the  $z$  - coordinate in the local cylindrical system, whereas,  $X_2 - X_3$  is the  $r - \theta$  plane, as shown in Figure 1. The indices  $j$  and  $p$  will be used as superscripts on all quantities to identify that particular quantity with the orientation of the composite assemblage element and the constituents within the element, respectively. However, for the sake of brevity in writing, they will be omitted unless needed for clarity. As a rule, a repeated subscript index will denote summation with respect to that index. However, a repeated supercript index will not imply summation. If we denote  $Q_{kn} = \cos(X_k, x_n),$  then from geometry in Figure 1, we have

$$Q_{km} = \begin{pmatrix} \cos \Omega & \sin \Omega \cos \phi & \sin \Omega \sin \phi \\ -\sin \Omega & \cos \Omega \cos \phi & \cos \Omega \sin \phi \\ 0 & -\sin \phi & \cos \phi \end{pmatrix} \quad (1)$$

### 3. BOUNDARY VALUE PROBLEM

The fiber, coating and the matrix are assumed to be linearly elastic, homogeneous and perfectly bonded. In general, the constituent materials may have transversely isotropic elastic and thermal expansion coefficients. Hence, the constitutive relations for each constituent material are given by

$$\begin{aligned} \sigma_z &= C_{11} (\epsilon_z - e_z) + C_{12} (\epsilon_r - e_r) + C_{12} (\epsilon_\theta - e_\theta) \\ \sigma_r &= C_{12} (\epsilon_z - e_z) + C_{22} (\epsilon_r - e_r) + C_{23} (\epsilon_\theta - e_\theta) \\ \sigma_\theta &= C_{12} (\epsilon_z - e_z) + C_{23} (\epsilon_r - e_r) + C_{22} (\epsilon_\theta - e_\theta) \\ \tau_{r\theta} &= C_{44} \gamma_{r\theta} \\ \tau_{z\theta} &= C_{55} \gamma_{z\theta} \\ \tau_{rz} &= C_{55} \gamma_{rz} \end{aligned} \quad (2)$$

where  $C_{mn}$  ( $m, n = 1, 2, \dots, 6$ ) are the elastic stiffness constants of the individual material and  $e_z$ ,  $e_r$  and  $e_\theta$  are the expansional (non-mechanical) strain components along the longitudinal ( $z$ ) and transverse directions ( $r - \theta$ ), respectively. In these relations the composite sphere model introduced by Hashin [11] can be employed to compute the effective properties of the particle reinforced matrix. Further, for a transversely isotropic material

$$\begin{aligned} e_r &= e_\theta \\ C_{44} &= 0.5 (C_{22} - C_{23}) \end{aligned} \quad (3)$$

In addition to (2), the elastic response of the constituents must satisfy the equilibrium equations

$$\sigma_{r,r} + \frac{1}{r} \tau_{r\theta,\theta} + \frac{1}{r} (\sigma_r - \sigma_\theta) = 0 \quad (4a)$$

$$\tau_{r\theta,r} + \frac{1}{r} \sigma_{\theta,\theta} + \frac{2}{r} \tau_{r\theta} = 0 \quad (4b)$$

$$\tau_{rz,r} + \frac{1}{r} \tau_{\theta z,\theta} + \frac{1}{r} \tau_{rz} = 0 \quad (4c)$$

where differentiation is indicated by a comma and the stresses are functions of  $r$  and  $\theta$  alone. The engineering strain-displacement relations are given by

$$\epsilon_z = u_{z,z}$$

$$\epsilon_r = u_{r,r}$$

$$\epsilon_\theta = \frac{1}{r} u_{\theta,\theta} + \frac{1}{r} u_r \quad (5)$$

$$\gamma_{r\theta} = \frac{1}{r} u_{r,\theta} + u_{\theta,r} - \frac{1}{r} u_\theta$$

$$\gamma_{\theta z} = u_{\theta,z} + \frac{1}{r} u_{z,\theta}$$

$$\gamma_{rz} = u_{r,z} + u_{z,r}$$

Substituting Eqs (2) and (5) into (4), the governing field equations for  $u_r$ ,  $u_\theta$  and  $u_z$  can be expressed as

$$C_{22} \left( u_{r,\pi} + \frac{1}{r} u_{r,r} - \frac{1}{r^2} u_r \right) + C_{44} \frac{1}{r^2} u_{r,\theta\theta} + (C_{23} + C_{44}) \frac{1}{r} u_{\theta,r\theta} - \quad (6a)$$

$$(C_{22} + C_{44}) \frac{1}{r^2} u_{\theta,\theta} + C_{12} u_{z,rz} = 0$$

$$C_{44} \left( u_{\theta,\pi} + \frac{1}{r} u_{\theta,r} - \frac{1}{r^2} u_\theta \right) + C_{22} \frac{1}{r^2} u_{\theta,\theta\theta} + (C_{23} + C_{44}) \frac{1}{r} u_{r,\theta} + \quad (6b)$$

$$(C_{22} + C_{44}) \frac{1}{r^2} u_{r,\theta} + C_{12} \frac{1}{r} u_{z,\theta z} = 0$$

$$C_{55} \left( u_{r,rz} + \frac{1}{r} u_{r,z} + \frac{1}{r} u_{\theta,z\theta} + u_{z,\pi} + \frac{1}{r} u_{z,r} + \frac{1}{r^2} u_{z,\theta\theta} \right) = 0 \quad (6c)$$

We now seek a solution of Eqs (6) subject to prescribed surface tractions. Let the composite material volume be now subjected to a set of boundary conditions of the form

$$T_i(S) = \sigma_{ik}^0 n_k \quad (7)$$

where  $n_k$  is the unit outward normal vector on the boundary surface  $S$ ,  $\sigma_{ik}^0$  are a set of constants and  $T_i$  denote the components of the boundary traction vector. For (7) prescribed, it can be shown that

$$\bar{\sigma}_{ik} = \sigma_{ik}^0 = \text{constant} \quad (8)$$

where an overbar denotes the average value over the whole volume.

To facilitate the analysis, we now introduce in Figure 2 an equivalent homogeneous medium, having the effective composite properties, as a comparison material. We further assume that the tractions acting on the radial boundary<sup>@</sup> of the composite cylinder elements,  $S_c$ , can be approximated by the boundary conditions of the equivalent material, i.e.,

$$\hat{T}_i^{(j)} = \bar{\sigma}_{ik}^{(j)} n_k \quad \text{on } S_c \quad (9)$$

where  $\hat{T}_i^{(j)}$  represents the traction components on the boundary of the  $j^{\text{th}}$  element in local coordinates;  $n_k^{(j)}$  is the unit outward normal vector on the boundary surface of the  $j^{\text{th}}$  element and  $\bar{\sigma}_{ik}^{(j)}$  are given by

$$\bar{\sigma}_{ik}^{(j)} = Q_{im}^{(j)} Q_{kn}^{(j)} \sigma_{mn}^0 \quad (j = 1, 2, \dots, N) \quad (10)$$

<sup>@</sup> Although Eq 9 is only applied on the radial boundary  $S_c$ , the validity of (8) for all stress components can be established for the present class of boundary value problems [12]

where the components of the transformation matrix  $Q_{kn}^{(j)}$  are defined in (1).

Thus, for a uniform state of stress applied to the composite volume, the boundary conditions on the surface of the cylindrical elements are independent of the axial coordinate. Beside those on the radial boundary, the complete specification of boundary conditions requires the prescription of the following resultants acting on any cross-section:

$$\begin{aligned}
 F_1 &= \int_0^{2\pi} \int_0^{r_3} \sigma_{zz} r \, dr \, d\theta \\
 M_1 &= \int_0^{2\pi} \int_0^{r_3} \tau_{z\theta} r^2 \, dr \, d\theta \\
 M_2 &= \int_0^{2\pi} \int_0^{r_3} \sigma_{zz} r^2 \sin \theta \, dr \, d\theta \\
 M_3 &= \int_0^{2\pi} \int_0^{r_3} \sigma_{zz} r^2 \cos \theta \, dr \, d\theta
 \end{aligned} \tag{11}$$

where  $F_1$  is the axial force;  $M_1$  the torque ; and  $M_2$  and  $M_3$  the resultant moment about the  $X_2$  and  $X_3$  axis, respectively. The four quantities, namely,  $F_1$ ,  $M_1$ ,  $M_2$  and  $M_3$  can be calculated from (10). The resultant forces in the  $X_2$  and  $X_3$  directions,  $F_2$  and  $F_3$  respectively, are non-zero, but do not provide independent information, e.g., the force component  $F_3$  is given by

$$F_3 = \int_0^{2\pi} \int_0^{r_3} ( \tau_{rz} \sin \theta + \tau_{z\theta} \cos \theta ) r \, dr \, d\theta \tag{12}$$

If we now multiply Eq (4c) by  $\sin \theta$  and, after a slight manipulation, substitute the results into (12), we find that

$$F_3 = \sum_{i=0}^2 \int_0^{2\pi} [ r_i^2 \tau_{rz}^i ]_{r_i}^{r_{i+1}} \sin \theta \, d\theta \tag{13}$$

Since  $\tau_{rz}$  is continuous at interfaces and  $r^2 \tau_{rz} = 0$  at the origin, this becomes

$$F_3 = \int_0^{2\pi} r_3^2 \tau_{rz}(r_3, \theta) \sin \theta \, d\theta \quad (14)$$

Thus,  $F_3$  is completely defined by the boundary conditions on  $r = r_3$  and cannot be independently prescribed. Similarly, it can be shown that

$$F_2 = \int_0^{2\pi} r_3^2 \tau_{rz}(r_3, \theta) \cos \theta \, d\theta \quad (15)$$

and cannot be arbitrarily prescribed if  $\tau_{rz}(r_3, \theta)$  is specified. Hence, the proper end conditions are the ones given by Eqs (11).

#### 4. GENERAL SOLUTION

We have three displacement fields (in materials (1), (2) and (3) or fiber, coating and matrix, respectively). The form of the governing field equations (6) and boundary conditions (9) and (11) lead to a general solution of the type

$$\begin{aligned} u_r(r, \theta, z) = & U_1^{(j,p)}(r) \cos 2\theta + U_2^{(j,p)}(r) \sin 2\theta + U_3^{(j,p)}(r) + U_4^{(j,p)}(r) \cos \theta + U_5^{(j,p)}(r) \sin \theta \\ & + U_6^{(j,p)}(r) z \cos \theta + U_7^{(j,p)}(r) z \sin \theta + U_8^{(j,p)}(r) z^2 \cos \theta + U_9^{(j,p)}(r) z^2 \sin \theta \end{aligned} \quad (16)$$

$$\begin{aligned} u_\theta(r, \theta, z) = & V_1^{(j,p)}(r) \sin 2\theta + V_2^{(j,p)}(r) \cos 2\theta + V_3^{(j,p)}(r) + V_4^{(j,p)}(r) \sin \theta + V_5^{(j,p)}(r) \cos \theta \\ & + V_6^{(j,p)}(r) z \sin \theta + V_7^{(j,p)}(r) z \cos \theta + V_8^{(j,p)}(r) z^2 \sin \theta + V_9^{(j,p)}(r) z^2 \cos \theta + z V_{10}^{(j,p)}(r) \end{aligned}$$

$$\begin{aligned}
u_z(r, \theta, z) = & \overset{(j, p)}{W_1(r)} \sin 2\theta + \overset{(j, p)}{W_2(r)} \cos 2\theta + \overset{(j, p)}{W_3(r)} + \overset{(j, p)}{W_4(r)} \sin \theta + \overset{(j, p)}{W_5(r)} \cos \theta \\
& + \overset{(j, p)}{W_6(r)} z \sin \theta + \overset{(j, p)}{W_7(r)} z \cos \theta + z \overset{(j, p)}{W_{10}(r)}
\end{aligned} \tag{16}$$

where  $j = 1, 2, \dots, N$ ;  $p = 1, 2, 3$  ;

and  $\overset{(j, p)}{U_1}(r), \overset{(j, p)}{U_2}(r) \dots, \overset{(j, p)}{W_{10}}(r)$  are defined in the Appendix.

A general solution of this form has been successfully employed by Pagano [13] to determine the stress field in a cylindrically anisotropic body under two-dimensional surface tractions. Using the strain-displacement equations (5) and the stress-strain relationships (2), the stress field is expressed as

$$\begin{aligned}
\sigma_z = & \overset{(j, p)}{\alpha_1}(r) \cos 2\theta + \overset{(j, p)}{\alpha_2}(r) \sin 2\theta + \overset{(j, p)}{\alpha_3}(r) + \overset{(j, p)}{\alpha_4}(r) \cos \theta + \overset{(j, p)}{\alpha_5}(r) \sin \theta \\
\sigma_r = & \overset{(j, p)}{\zeta_1}(r) \cos 2\theta + \overset{(j, p)}{\zeta_2}(r) \sin 2\theta + \overset{(j, p)}{\zeta_3}(r) + \overset{(j, p)}{\zeta_4}(r) \cos \theta + \overset{(j, p)}{\zeta_5}(r) \sin \theta \\
\sigma_\theta = & \overset{(j, p)}{\beta_1}(r) \cos 2\theta + \overset{(j, p)}{\beta_2}(r) \sin 2\theta + \overset{(j, p)}{\beta_3}(r) + \overset{(j, p)}{\beta_4}(r) \cos \theta + \overset{(j, p)}{\beta_5}(r) \sin \theta \\
\tau_{r\theta} = & \overset{(j, p)}{\gamma_1}(r) \sin 2\theta + \overset{(j, p)}{\gamma_2}(r) \cos 2\theta + \overset{(j, p)}{\gamma_3}(r) + \overset{(j, p)}{\gamma_4}(r) \sin \theta + \overset{(j, p)}{\gamma_5}(r) \cos \theta \\
\tau_{\theta z} = & \overset{(j, p)}{\xi_1}(r) \cos 2\theta + \overset{(j, p)}{\xi_2}(r) \sin 2\theta + \overset{(j, p)}{\xi_3}(r) + \overset{(j, p)}{\xi_4}(r) \cos \theta + \overset{(j, p)}{\xi_5}(r) \sin \theta \\
\tau_{rz} = & \overset{(j, p)}{\delta_1}(r) \sin 2\theta + \overset{(j, p)}{\delta_2}(r) \cos 2\theta + \overset{(j, p)}{\delta_3}(r) + \overset{(j, p)}{\delta_4}(r) \sin \theta + \overset{(j, p)}{\delta_5}(r) \cos \theta
\end{aligned} \tag{17}$$

where  $\overset{(j, p)}{\alpha_1}(r), \overset{(j, p)}{\alpha_2}(r) \dots, \overset{(j, p)}{\delta_3}(r), \overset{(j, p)}{\delta_4}(r), \overset{(j, p)}{\delta_5}(r)$  are defined in the Appendix. The constants

$\overset{(j, p)}{A_1}, \overset{(j, p)}{A_2} \dots, \overset{(j, p)}{Y_2}, \overset{(j, p)}{Y_3}$  used to define the coefficients  $\overset{(j, p)}{U_1}(r) \dots \overset{(j, p)}{W_{10}}(r)$  in Eqs (16) and  $\overset{(j, p)}{\alpha_1}(r) \dots \overset{(j, p)}{\delta_5}(r)$

in Eqs (17) are to be evaluated by the following interface/boundary conditions :

i) Displacements and traction must be continuous across the fiber-coating and coating-matrix interfaces, which lead to the following equations :

$$\begin{aligned} {}^{(j,1)}P_k(r_1) &= {}^{(j,2)}P_k(r_1) \\ {}^{(j,2)}P_k(r_2) &= {}^{(j,3)}P_k(r_2) \end{aligned} \quad \begin{array}{l} (k = 1, 2, \dots, 10) \\ (j = 1, 2, \dots, N) \end{array} \quad (18)$$

where  $P = U, V, W, \zeta, \gamma$  and  $\delta$  if  $k = 1, 2, 3, 4, 5$   
 $P = U$  if  $k = 6, 7, 8, 9$   
 $P = V, W$  if  $k = 10$

ii) To avoid singularities, displacements and stresses must be bounded at the origin which results in the following relations for  $j = 1, 2, \dots, N$  :

$$\begin{aligned} {}^{(j,1)}A_2 = {}^{(j,1)}A_4 = 0; \quad {}^{(j,1)}B_2 = {}^{(j,1)}B_4 = 0; \\ {}^{(j,1)}P_2 = {}^{(j,1)}P_4 = 0; \quad {}^{(j,1)}Q_2 = {}^{(j,1)}Q_4 = 0; \\ {}^{(j,1)}D_2 = {}^{(j,1)}F_2 = {}^{(j,1)}H_2 = {}^{(j,1)}S_2 = {}^{(j,1)}T_2 = {}^{(j,1)}X_2 = {}^{(j,1)}Y_2 = 0. \end{aligned} \quad (19)$$

iii) For convenience, we neglect the displacements reflecting rigid body motion, which implies that

$${}^{(j,p)}F_1 = {}^{(j,p)}H_1 = {}^{(j,p)}P_5 = {}^{(j,p)}Q_5 = {}^{(j,p)}X_3 = {}^{(j,p)}Y_3 = 0. \quad \begin{array}{l} (j = 1, 2, \dots, N) \\ (p = 1 \text{ or } 2 \text{ or } 3) \end{array} \quad (20)$$

within any one constituent.

iv) Boundary conditions are prescribed over the cross-section (Eqs 11) and on the radial surface (Eq 9) of the cylindrical elements. Equilibrium of the entire body, however, imposes certain implied connections among the traction components, e.g, consider the portion of the solution in which the stress field is represented by the following components [13]:

$$\begin{aligned}
\sigma_r(r, \theta) &= \sigma_r^*(r) \cos \theta \\
\sigma_\theta(r, \theta) &= \sigma_\theta^*(r) \cos \theta \\
\tau_{r\theta}(r, \theta) &= \tau_{r\theta}^*(r) \sin \theta
\end{aligned}
\tag{21}$$

Putting these functions into (4a) and (4b) and eliminating  $\sigma_\theta^*(r)$  establishes the relation

$$\frac{d}{dr} [r \sigma_r^*(r)] = \frac{d}{dr} [r \tau_{r\theta}^*(r)]
\tag{22}$$

which, on integration over the cross-section becomes

$$r_3 [\sigma_r^*(r_3) - \tau_{r\theta}^*(r_3)] = 0
\tag{23}$$

since tractions are continuous at the interfaces. Reversing  $\cos \theta$  and  $\sin \theta$  also leads to an equation of the form of (23). Hence, the coefficients of the terms involving  $\sin \theta$  and  $\cos \theta$ , given by the prescribed traction components (Eq 9), are constrained by Eq 23. No other terms in the solution lead to constraints of this type.

## 5. THE COMPOSITE RESPONSE

Under prescribed traction, the solution to the displacement and the stress field within the constituents of the composite cylinder assemblage is given by Eqs (16) and (17), respectively, as discussed earlier. The composite mathematical strain can be determined by volume averaging the strain field over the constituents, namely, the composite cylinder elements and the interstitial matrix. The stress-strain relation for the composite now takes the form (using contracted notation)

$$\bar{\epsilon}_m = \bar{S}_{mn} \bar{\sigma}_n + \bar{e}_m \quad (m, n = 1, 2, \dots, 6)
\tag{24}$$

where  $\bar{S}_{mn}$  is the effective compliance;  $\bar{e}_m$  is the effective expansional (non-mechanical) strain of the composite and  $\bar{\sigma}_n = \sigma_n^0$ .

To evaluate the effective elastic moduli, we set the expansional strain components identically equal to zero, i.e.,

$$\overset{(j,p)}{e_m} = 0 \quad (\text{for all } j, p)$$

The stress-strain relation for the composite, Eq (24), therefore reduces to

$$\bar{e}_m = \bar{S}_{mn} \bar{\sigma}_n$$

By setting each stress component equal to one individually, while all others are zero, we will respectively obtain the  $n^{\text{th}}$  column of the  $\bar{S}_{mn}$  matrix. The composite engineering constants can now be defined in terms of the elastic compliances.

The expansional strains of a body subjected to thermo-mechanical loading can be computed in the following manner :

Consider the case where the local material expansional strains are given their actual values according to some external stimulus, such as a temperature change. Suppose we set  $\bar{\sigma}_n = 0$ . Then, from Eq. (24), we have

$$\bar{e}_m = \bar{e}_m$$

where the composite mathematical strain  $\bar{e}_m$  can be computed as explained earlier.

## 6. NUMERICAL RESULTS AND DISCUSSION

The use of displacement or traction boundary conditions on the surface of the composite cylinder element in conjunction with the approach described in this work leads to bounding solutions for the composite effective moduli. Our earlier study [10] reported results based on displacement boundary conditions which lead to an upper bound of the elastic stiffnesses. In this paper, we have considered traction boundary conditions on the surface of the composite cylinder element. This

approach leads to a lower bound estimate of the composite effective moduli and together with the upper bound results provides a more precise estimate of the composite properties. The composite cylinder assemblage model is, of course, a geometric idealization of a real fiber reinforced material. We will first present the bounding solutions for the effective thermo-elastic moduli for unidirectional Graphite/Epoxy and Nicalon/BMAS (Barium Magnesium Aluminosilicate) composite systems. The Graphite fiber is assumed to be transversely isotropic while the Nicalon fiber and Epoxy and BMAS matrices are assumed to be isotropic in nature. The material properties used in the calculations are listed as follows :

Graphite fiber :  $E_T = 9.66 \text{ GPa}$  ;  $E_A = 345 \text{ GPa}$  ;  $G_A = 2.07 \text{ GPa}$  ;  $\nu_T = 0.29$  ;  
 $\nu_A = 0.20$  ;  $\alpha_T = 9.0 \times 10^{-6} / ^\circ\text{C}$  ;  $\alpha_A = - 0.36 \times 10^{-6} / ^\circ\text{C}$  ;

Nicalon fiber :  $E = 200 \text{ GPa}$  ;  $G = 77 \text{ GPa}$  ;  $\alpha = 3.2 \times 10^{-6} / ^\circ\text{C}$  ;

Epoxy matrix :  $E = 3.456 \text{ GPa}$  ;  $G = 1.28 \text{ GPa}$  ;  $\alpha = 40.9 \times 10^{-6} / ^\circ\text{C}$  ;

BMAS matrix :  $E = 106 \text{ GPa}$  ;  $G = 43 \text{ GPa}$  ;  $\alpha = 2.7 \times 10^{-6} / ^\circ\text{C}$  ;

With the fibers aligned unidirectionally (along  $x_1$ ), the composite is transversely isotropic and has five independent elastic constants. These can be expressed as longitudinal Young's modulus,  $E_{11}$  ; major Poisson's ratio,  $\nu_{12}$  ; longitudinal shear modulus,  $G_{12}$  ; plane-strain bulk modulus,  $K_{23}$  ; and transverse Young's modulus,  $E_{22}$  . The thermal expansion coefficients in the longitudinal and transverse directions are denoted by  $\alpha_{11}$  and  $\alpha_{22}$  , respectively.

The effective moduli solutions for the two material systems, at different fiber volume fractions, are listed in Table 1. Upper and lower bounds for four of the five elastic moduli, namely,  $E_{11}$  ,  $\nu_{12}$  ,  $G_{12}$  and  $K_{23}$  coincide whereas, bounding solutions for the fifth modulus,  $E_{22}$  , are obtained. The  $E_{22}$  bounds for the two material systems under study are, however, very close to each other. This is due to the closeness of the transverse moduli of the constituents in each case. Thus, the range of effective property prediction is indeed tight. The BMAS matrix with a relatively larger value of

Young's modulus leads to much higher estimates of composite  $E_{22}$  as compared to the softer epoxy matrix. Since the Graphite fiber has a large ratio of  $E_A / E_T$ , the stiffening effect for the Graphite/Epoxy composite is much more pronounced in the longitudinal direction as compared to that in the transverse direction. Such strong directionality effects are not observed for the Nicalon/BMAS system since the Nicalon fiber is assumed to be isotropic. For uncoated fibers, the moduli results derived by Hashin and Rosen [14] are recovered.

The solution for the effective thermal expansion coefficients of Graphite/Epoxy and Nicalon/BMAS composite systems are illustrated in Figures 3 (a) and 3 (b), respectively. Upper and lower bounds for both the longitudinal and transverse coefficients are seen to coincide and Levin's solution [15] is recovered for an uncoated fibrous composite. Low expansions are obtained in the axial direction for Graphite/Epoxy because of the low expansion coefficient of the fiber. The initial increase in transverse expansion coefficient for Graphite/Epoxy system is probably due to the axial restraint of the fiber. This phenomenon where the composite transverse expansion coefficient increases above that of its constituents expansion coefficients is being examined elsewhere [16]. No such phenomenon is observed for the isotropic Nicalon fiber and BMAS matrix system.

We will next consider the effect of different coating materials and thicknesses on the behavior of a three-dimensional fibrous composite obtained by arranging six fibers parallel to the six lines joining the opposite vertices of a regular icosahedron. These six axes can be oriented with reference to an orthogonal cartesian coordinate system  $x_1 x_2 x_3$  as follows : one pair in the  $x_1 x_2$  plane making angles of  $\theta'$  with the  $x_1$ -axis, one pair in the  $x_2 x_3$  plane making angles of  $\theta'$  with the  $x_2$ -axis, and one pair in the  $x_3 x_1$  plane making angles of  $\theta'$  with the  $x_3$ -axis, where  $\theta' = \tan^{-1}(2 \sin 18^\circ) = 31^\circ 43'$ . As shown by Rosen and Shu [17], this type of arrangement gives rise to local isotropy. The isotropic relation  $G = E / [ 2 ( 1 + \nu ) ]$  can be used as an independent

check of the model. In general, this relation is not satisfied exactly in the present analysis, however the error is very small.

The bounding solutions for the Nicalon fiber and BMAS matrix system are shown in Table 2. Also shown in the table is the effect of different coating thicknesses and coating materials on the effective thermoelastic moduli. The fiber volume fraction was set at 30% but the ratio of coating thickness to the cylinder outer radius, defined as  $(r_2 - r_1) / r_3$ , was treated as an independent variable. The material properties of the two coating materials used in the calculations were :

<u>Coating Material</u>	<u>E (GPa)</u>	<u>G (GPa)</u>	<u><math>\alpha</math> (<math>10^{-6} / ^\circ\text{C}</math>)</u>
Nickel	207	79	13.3
ATJS, Carbon	9.1	4.1	2.2

As seen from Table 2, the bounds for the effective thermoelastic moduli do not coincide and the gap between them increases as the coating thickness is increased.

The microstress distribution within the constituents of a multidirectional fiber composite, in general, depends both on the type of loading and the fiber orientation. Here we consider as an example the curing stresses in such a body. As an approximation, the curing or residual stresses can be estimated by subjecting the composite to a uniform temperature change. For the specific three-dimensional composite under consideration, the stress distribution is identical for the six fiber orientations. In this problem, the only non-zero stress components predicted by the present model are  $\sigma_r$ ,  $\sigma_\theta$  and  $\sigma_z$ . The stress concentration is a function of both Young's modulus and the thermal expansion coefficient of the coating, besides its thickness. The effect of different coating materials and/or thicknesses on the stress concentrations is quite dramatic. These trends are illustrated for both the displacement and traction formulations in Tables 3(a), 3(b) and 3(c) for the components  $\sigma_r$ ,  $\sigma_\theta$  and  $\sigma_z$ , respectively, where a 1  $^\circ\text{C}$  temperature drop is imposed.

The radial stress component at the interface can be considered as a failure criteria for debonding, e.g., a negative value of  $\sigma_r$  promotes contact between the constituents, whereas, a positive value suggests possible initiation of debonding and separation at the boundary. It is seen that a 'thick' coating of a 'soft' material with a 'low' coefficient of thermal expansion helps in reducing the stress concentration factor at the boundary. Within the coating, the algebraic maximum hoop stress occurs at the fiber-coating interface, whereas, in the matrix, the maximum occurs at the coating-matrix interface. It is this maximum value of hoop stress which is listed in Table 3(b). The present model predicts the longitudinal stress component,  $\sigma_z$ , to be a constant within each one of the constituents. It is seen that extremely large tensile stresses develop in the Nickel coating which has a high coefficient of thermal expansion whereas, carbon coating, with a low value of E and  $\alpha$ , helps in reducing the stress concentration both in the fiber as well as in the matrix.

To conclude, it is apparent that generally a reduction in the stress concentration can be made at the expense of the elastic moduli of the composite. Further, by a proper choice of coating thickness, modulus and coefficient of thermal expansion, the stress component of interest, which is instrumental in causing a specific mode of failure, can be controlled.

## 7. THE NDSANDS PROGRAM

Micromechanical considerations in composite materials may require the use of a practical tool that can handle different constituent materials, arbitrary fiber orientations and multi-axial loading conditions. To address these requirements, the computer code called NDSANDS (N Directional Stiffness A ND Strength), developed earlier for displacement boundary conditions [10], has been modified to account for prescribed surface tractions. It can be used either to analyze a composite or to conduct a parametric study. By parametric study is meant that the user can change either a material property or the geometry of the composite, one single variable at a time while the remainder are kept constant, and thereby examine the change in effective properties and stress

distribution as a result of different input values of the parameter selected. When changing the material property, we must insure that both the stiffness and compliance matrices remain positive definite at all times [18]. Although we have presented the formulation here for only one coating, as many as five coating regions can be modeled in the code.

## 8. SUMMARY

In summary, we have developed a first order ideal material model to approximate the thermo-elastic response of a composite body reinforced by coated fibers oriented in various directions. The coating can either be applied intentionally to achieve the desirable composite properties or it can occur as a consequence of the processing conditions involved in the composite manufacture. This formulation corresponding to prescribed surface tractions on the boundary of the representative volume element leads to a lower bound calculation of the effective moduli and together with the upper bound results [10] provides a more precise estimate of the composite properties. Parametric studies have been further conducted to demonstrate the effect of coating materials and thicknesses on the overall behavior of a three-dimensional fibrous composite.

## REFERENCES

1. B. Bender, D. Shadwell, C. Bulik, L. Incorvati and D. Lewis, 'Effect of Fiber Coatings and Composite Processing on Properties of Zirconia - Based Matrix SiC Fiber Composites', *Ceramic Bulletin*, 65 [2] (1986) pp 363-369
2. R. N. Singh and M. K. Brun, 'Effect of Boron Nitride Coating on Fiber-Matrix Interactions', *Ceram. Eng. Sci. Proc.*, 8 [7-8] (1987) pp 636-643
3. M. K. Brun and R. N. Singh, 'Effect of Thermal Expansion Mismatch and Fiber Coatings on the Fiber/Matrix Interfacial Shear Stress in Ceramic Matrix Composites', *Adv. Cer. Matls.*, 3 [5] (1988) pp 506-509

4. A. G. Atkins, 'Intermittent Bonding for High Toughness / High Strength Composites', *J. Mat. Sci.*, 10 (1975) pp 819-832
5. H. L. Hancox and H. Wells, 'The Effect of Fiber Surface Coatings on the Mechanical Properties of CFRP', *Fibre Sci & Techn.*, 10 (1977) pp 9-22
6. J. H. Williams, Jr. and P. N. Kousiounelos, 'Thermoplastic Fiber Coatings Enhance Composite Strength and Toughness', *Fibre Sci & Techn.*, 11 (1978) pp 83-88
7. D. F. Adams, 'A Micromechanical Analysis of the Influence of the Interface on the Performance of Polymer-Matrix Composites', *Proc. Amer. Soc. for Comp.*, First Technical Conference (1986) pp 207-226
8. Y. Mikata and M. Taya, 'Stress Field in a Coated Continuous Fiber Composite Subjected to Thermo-Mechanical Loadings', *J. Comp. Matl.*, 19 (1985) pp 554-579
9. S. N. Chatterjee and J. J. Kibler, 'An Analytical Model for Three - Dimensionally Reinforced Graphite Composites', in Modern Developments in Composite Materials and Structures, (1979) pp 269-287
10. N. J. Pagano and G. P. Tandon, 'Elastic Response of Multidirectional Coated Fiber Composites', *Comp. Sci. & Tech.*, 31 (1988) pp 273-293
11. Z. Hashin, 'The Elastic Moduli of Heterogeneous Materials', *J. Appl. Mech.*, 29 (1962) pp 143-150
12. N. J. Pagano and G. P. Tandon (to be published)
13. N. J. Pagano, 'The Stress Field in a Cylindrically Anisotropic Body Under Two-Dimensional Surface Traction', *J. Appl. Mech.*, 39 (1972) pp. 791-796
14. Z. Hashin and B. W. Rosen, 'The Elastic Moduli of Fiber Reinforced Materials', *J. Appl. Mech.*, 31 (1964) pp 223-232
15. V. M. Levin, 'On the Coefficients of Thermal Expansion of Heterogeneous Materials', *Mech. of Solids*, 2 (1967) pp 58-61

16. A. Chatterjee, G. P. Tandon and L. E. Matson, ' Anomalous Expansion Behavior in Ceramic Fiber Reinforced Brittle Matrix Composites ', to be presented at Symposium on High Temperature Composites , Dayton, OH, June 13 - 15 (1989)
17. B. W. Rosen and L. S. Shu, ' On Some Symmetry Conditions For Three - Dimensional Fibrous Composites ', J. Comp. Matl., 5 (1972) pp 279-282
18. R. M. Jones, Mechanics of Composite Materials , McGraw - Hill book Company, New York (1975) pp 37-45

## APPENDIX

$$U_1(r) = A_1 r^3 + \frac{A_2}{r^3} + A_3 r + \frac{A_4}{r}$$

$$V_1(r) = - \frac{(3 C_{22} + C_{23})}{2 C_{23}} A_1 r^3 + \frac{A_2}{r^3} - A_3 r - \frac{(C_{22} - C_{23})}{2 C_{22}} \frac{A_4}{r}$$

$$W_1(r) = S_1 r^2 + \frac{S_2}{r^2}$$

$$U_2(r) = B_1 r^3 + \frac{B_2}{r^3} + B_3 r + \frac{B_4}{r}$$

$$V_2(r) = \frac{(3 C_{22} + C_{23})}{2 C_{23}} B_1 r^3 - \frac{B_2}{r^3} + B_3 r + \frac{(C_{22} - C_{23})}{2 C_{22}} \frac{B_4}{r}$$

$$W_2(r) = T_1 r^2 + \frac{T_2}{r^2}$$

$$U_3(r) = D_1 r + \frac{D_2}{r}$$

$$V_3(r) = F_1 r + \frac{F_2}{r}$$

$$W_3(r) = H_1 + H_2 \ln r$$

$$U_4(r) = \left[ \frac{2 C_{12}}{5 C_{22} + C_{23}} P_3 + P_1 \right] r^2 + \frac{P_2}{r^2} + P_4 \ln r + P_5$$

$$V_4(r) = \frac{(5 C_{22} + C_{23})}{C_{22} - 3 C_{23}} P_1 r^2 + \frac{P_2}{r^2} - P_4 \left[ \ln r + \frac{(C_{22} + C_{23})}{3 C_{22} - C_{23}} \right] - P_5$$

$$W_4(r) = (X_1 + X_3) r + \frac{X_2}{r}$$

$$U_5(r) = \left[ - \frac{2 C_{12}}{5 C_{22} + C_{23}} Q_3 + Q_1 \right] r^2 + \frac{Q_2}{r^2} + Q_4 \ln r + Q_5$$

$$V_5(r) = - \frac{(5 C_{22} + C_{23})}{C_{22} - 3 C_{23}} Q_1 r^2 - \frac{Q_2}{r^2} + Q_4 \left[ \ln r + \frac{(C_{22} + C_{23})}{3 C_{22} - C_{23}} \right] + Q_5$$

$$W_5(r) = (Y_1 - Y_3) r + \frac{Y_2}{r}$$

$$U_6(r) = -V_6(r) = Y_3$$

$$W_6(r) = Q_3 r$$

$$U_7(r) = V_7(r) = -X_3$$

$$W_7(r) = -P_3 r$$

$$U_8(r) = -V_8(r) = 0.5 P_3$$

$$U_9(r) = V_9(r) = -0.5 Q_3$$

$$V_{10}(r) = F_3 r$$

$$W_{10}(r) = D_3$$

$$\alpha_1(r) = C_{12} (C_{23} - C_{22}) \left\{ \frac{3 A_1 r^2}{C_{23}} + \frac{A_4}{C_{22} r^2} \right\}$$

$$\zeta_1(r) = (C_{22} - C_{23}) \left\{ -\frac{3 A_2}{r^4} + A_3 - \frac{(C_{22} + C_{23})}{C_{22}} \frac{A_4}{r^2} \right\}$$

$$\beta_1(r) = (C_{22} - C_{23}) \left\{ -\frac{3(C_{22} + C_{23})}{C_{23}} A_1 r^2 + \frac{3 A_2}{r^4} - A_3 \right\}$$

$$\gamma_1(r) = 0.5 (C_{22} - C_{23}) \left\{ -\frac{3(C_{22} + C_{23})}{C_{23}} A_1 r^2 - \frac{6 A_2}{r^4} - 2 A_3 - \frac{(C_{22} + C_{23})}{C_{22}} \frac{A_4}{r^2} \right\}$$

$$\xi_1(r) = 2 C_{55} \left\{ S_1 r + \frac{S_2}{r^3} \right\}$$

$$\delta_1(r) = 2 C_{55} \left\{ S_1 r - \frac{S_2}{r^3} \right\}$$

$$\alpha_2(r) = C_{12} (C_{23} - C_{22}) \left\{ \frac{3 B_1 r^2}{C_{23}} + \frac{B_4}{C_{22} r^2} \right\}$$

$$\zeta_2(r) = (C_{22} - C_{23}) \left\{ -\frac{3 B_2}{r^4} + B_3 - \frac{(C_{22} + C_{23})}{C_{22}} \frac{B_4}{r^2} \right\}$$

$$\beta_2(r) = (C_{22} - C_{23}) \left\{ -\frac{3(C_{22} + C_{23})}{C_{23}} B_1 r^2 + \frac{3 B_2}{r^4} - B_3 \right\}$$

$$\gamma_2(r) = 0.5 (C_{22} - C_{23}) \left( \frac{3(C_{22} + C_{23})}{C_{23}} B_1 r^2 + \frac{6 B_2}{r^4} + 2 B_3 + \frac{(C_{22} + C_{23})}{C_{22}} \frac{B_4}{r^2} \right)$$

$$\xi_2(r) = -2 C_{55} \left( T_1 r + \frac{T_2}{r^3} \right)$$

$$\delta_2(r) = 2 C_{55} \left( T_1 r - \frac{T_2}{r^3} \right)$$

$$\alpha_3(r) = C_{11} (D_3 - e_z) + 2 C_{12} (D_1 - e_r)$$

$$\zeta_3(r) = C_{12} (D_3 - e_z) + (C_{22} + C_{23}) (D_1 - e_r) - (C_{22} - C_{23}) \frac{D_2}{r^2}$$

$$\beta_3(r) = C_{12} (D_3 - e_z) + (C_{22} + C_{23}) (D_1 - e_r) + (C_{22} - C_{23}) \frac{D_2}{r^2}$$

$$\gamma_3(r) = -2 C_{44} \frac{F_2}{r^2}$$

$$\xi_3(r) = C_{55} F_3 r$$

$$\delta_3(r) = C_{55} \frac{H_2}{r}$$

$$\alpha_4(r) = \left\{ \frac{8 C_{12} (C_{22} - C_{23})}{C_{22} - 3 C_{23}} P_1 + \left[ -C_{11} + \frac{6 C_{12}^2}{5 C_{22} + C_{23}} \right] P_3 \right\} r + \frac{2 C_{12} (C_{22} - C_{23})}{3 C_{22} - C_{23}} \frac{P_4}{r}$$

$$\zeta_4(r) = (C_{22} - C_{23}) \left\{ \left[ \frac{2(C_{22} + C_{23})}{C_{22} - 3 C_{23}} P_1 - \frac{C_{12}}{5 C_{22} + C_{23}} P_3 \right] r - \frac{2 P_2}{r^3} + \frac{3 C_{22} + C_{23}}{3 C_{22} - C_{23}} \frac{P_4}{r} \right\}$$

$$\beta_4(r) = (C_{22} - C_{23}) \left\{ \left[ \frac{6(C_{22} + C_{23})}{C_{22} - 3 C_{23}} P_1 - \frac{3 C_{12}}{5 C_{22} + C_{23}} P_3 \right] r + \frac{2 P_2}{r^3} - \frac{C_{22} - C_{23}}{3 C_{22} - C_{23}} \frac{P_4}{r} \right\}$$

$$\gamma_4(r) = 0.5 (C_{22} - C_{23}) \left\{ \left[ \frac{4(C_{22} + C_{23})}{C_{22} - 3C_{23}} P_1 - \frac{2C_{12}}{5C_{22} + C_{23}} P_3 \right] r - \frac{4P_2}{r^3} - \frac{2(C_{22} - C_{23})}{3C_{22} - C_{23}} \frac{P_4}{r} \right\}$$

$$\xi_4(r) = C_{55} \left\{ X_1 + \frac{X_2}{r^2} \right\}$$

$$\delta_4(r) = C_{55} \left\{ X_1 - \frac{X_2}{r^2} \right\}$$

$$\alpha_5(r) = \left\{ \frac{8C_{12}(C_{22} - C_{23})}{C_{22} - 3C_{23}} Q_1 + \left[ C_{11} - \frac{6C_{12}^2}{5C_{22} + C_{23}} \right] Q_3 \right\} r + \frac{2C_{12}(C_{22} - C_{23})}{3C_{22} - C_{23}} \frac{Q_4}{r}$$

$$\zeta_5(r) = (C_{22} - C_{23}) \left\{ \left[ \frac{2(C_{22} + C_{23})}{C_{22} - 3C_{23}} Q_1 + \frac{C_{12}}{5C_{22} + C_{23}} Q_3 \right] r - \frac{2Q_2}{r^3} + \frac{3C_{22} + C_{23}}{3C_{22} - C_{23}} \frac{Q_4}{r} \right\}$$

$$\beta_5(r) = (C_{22} - C_{23}) \left\{ \left[ \frac{6(C_{22} + C_{23})}{C_{22} - 3C_{23}} Q_1 + \frac{3C_{12}}{5C_{22} + C_{23}} Q_3 \right] r + \frac{2Q_2}{r^3} - \frac{C_{22} - C_{23}}{3C_{22} - C_{23}} \frac{Q_4}{r} \right\}$$

$$\gamma_5(r) = 0.5 (C_{22} - C_{23}) \left\{ \left[ -\frac{4(C_{22} + C_{23})}{C_{22} - 3C_{23}} Q_1 - \frac{2C_{12}}{5C_{22} + C_{23}} Q_3 \right] r + \frac{4Q_2}{r^3} + \frac{2(C_{22} - C_{23})}{3C_{22} - C_{23}} \frac{Q_4}{r} \right\}$$

$$\xi_5(r) = -C_{55} \left\{ Y_1 + \frac{Y_2}{r^2} \right\}$$

$$\delta_5(r) = C_{55} \left( Y_1 - \frac{Y_2}{r^2} \right)$$

where  $A_1, A_2, \dots, Y_3$  are constants. Each one of the constants and the elastic coefficients have a superscript  $(j, p)$  where  $j$  identifies that quantity with the orientation of the composite cylinder element and  $p$  identifies the material constituent within that element. Further, in the equations listed above,  $r$  is a variable with the following limits :

$$\begin{aligned} \text{if } p = 1, & \quad 0 \leq r \leq r_1^{(j)} \\ \text{if } p = 2, & \quad r_1^{(j)} \leq r \leq r_2^{(j)} \\ \text{if } p = 3, & \quad r_2^{(j)} \leq r \leq r_3^{(j)} \end{aligned} \quad , \quad j = 1, 2, \dots, N$$

**TABLE 1 . Effective elastic properties for unidirectional Graphite/Epoxy and Nicalon/BMAS composite systems**

Composite System	$v_f$	$E_{11}$ (GPa)	$v_{12}$	$G_{12}$ (GPa)	$K_{23}$ (GPa)	$E_{22}$ (GPa)	
						Upper	Lower
Graphite/Epoxy	0.0	3.46	0.350	1.28	4.27	3.456	3.456
	0.2	71.78	0.318	1.41	4.65	4.634	4.507
	0.4	140.12	0.287	1.55	5.09	5.579	5.227
	0.6	208.41	0.257	1.70	5.60	6.671	6.227
	0.8	276.69	0.228	1.88	6.20	7.947	7.688
	1.0	345.00	0.200	2.07	6.91	9.660	9.660
	Nicalon/BMAS	0.0	106.00	0.233	43.00	80.40	106.00
0.2		124.89	0.248	48.17	93.30	119.20	118.47
0.4		143.74	0.263	53.99	109.21	134.77	132.83
0.6		162.53	0.276	60.62	129.33	152.84	150.55
0.8		181.28	0.288	68.21	155.58	174.03	172.82
1.0		200.00	0.299	77.00	191.26	200.00	200.00

**TABLE 2 . Effective thermo-elastic moduli for three-dimensional ' isotropic ' composite**

Coating thickness Cylinder outer radius	Composite system	Formulation	E (GPa)	G (GPa)	$\nu$	$\alpha$ ( $10^{-6}/^{\circ}\text{C}$ )
0.00	Nicalon/BMAS	Displacement	128.16	51.25	0.250	2.8896
		Traction	127.35	50.87	0.252	2.8891
0.01	Nicalon/Nickel/ BMAS	Displacement	129.11	51.60	0.251	3.0415
		Traction	128.25	51.20	0.253	3.0404
	Nicalon/Carbon/ BMAS	Displacement	118.06	47.50	0.243	2.8787
		Traction	117.49	47.27	0.243	2.8767
0.10	Nicalon/Nickel/ BMAS	Displacement	138.72	55.10	0.259	4.4549
		Traction	137.50	54.54	0.261	4.4496
	Nicalon/Carbon/ BMAS	Displacement	80.200	32.94	0.217	2.8410
		Traction	74.960	30.76	0.218	2.8243

**TABLE 3 (a) . Stress component  $\sigma_r$  in the fiber-coating and coating-matrix interface for  $\Delta T = -1^\circ C$**

coating thickness cylinder outer radius	Composite system	Formulation	$(\sigma_r)_{f-c}$ (KPa)	$(\sigma_r)_{c-m}$ (KPa)
0	Nicalon/BMAS	Displacement	26.4	26.4
		Traction	29.0	29.0
0.01	Nicalon/Nickel/ BMAS	Displacement	-8.98	44.9
		Traction	-4.37	49.5
	Nicalon/Carbon/ BMAS	Displacement	22.8	22.3
		Traction	25.8	25.2
0.10	Nicalon/Nickel/ BMAS	Displacement	-290.0	140.0
		Traction	-269.0	160.0
	Nicalon/Carbon/ BMAS	Displacement	8.54	5.95
		Traction	12.40	9.40

**TABLE 3 (b) . Stress component  $\sigma_\theta$  (algebraic maximum) in the fiber, coating and matrix for  $\Delta T = -1^\circ C$**

coating thickness cylinder outer radius	Composite system	Formulation	$(\sigma_\theta)_f$ (KPa)	$(\sigma_\theta)_c$ (KPa)	$(\sigma_\theta)_m$ (KPa)
0	Nicalon/BMAS	Displacement	26.4	-	-55.6
		Traction	29.0	-	-53.8
0.01	Nicalon/Nickel/ BMAS	Displacement	-8.98	3020.0	-97.5
		Traction	-4.37	3030.0	-94.1
	Nicalon/Carbon/ BMAS	Displacement	22.8	-7.46	-50.7
		Traction	25.8	-6.93	-47.9
0.10	Nicalon/Nickel/ BMAS	Displacement	-290.0	2720.0	-407.0
		Traction	-269.0	2740.0	-392.0
	Nicalon/Carbon/ BMAS	Displacement	8.54	-9.63	-32.0
		Traction	12.4	-8.88	-23.0

**TABLE 3 (c). Stress component  $\sigma_z$  in the fiber, coating and matrix for  $\Delta T = -1^{\circ} C$**

coating thickness cylinder outer radius	Composite system	Formulation	$(\sigma_z)_f$ (KPa)	$(\sigma_z)_c$ (KPa)	$(\sigma_z)_m$ (KPa)
0	Nicalon/BMAS	Displacement	77.9	-	-26.9
		Traction	70.9	-	-30.4
0.01	Nicalon/Nickel/ BMAS	Displacement	26.3	3060.0	-48.4
		Traction	13.6	3040.0	-54.8
	Nicalon/Carbon/ BMAS	Displacement	77.9	-4.52	-25.5
		Traction	68.9	-4.63	-29.9
0.10	Nicalon/Nickel/ BMAS	Displacement	-424.0	2590.0	-248.0
		Traction	-477.0	2530.0	-275.0
	Nicalon/Carbon/ BMAS	Displacement	76.9	-5.99	-21.0
		Traction	58.7	-6.41	-29.0

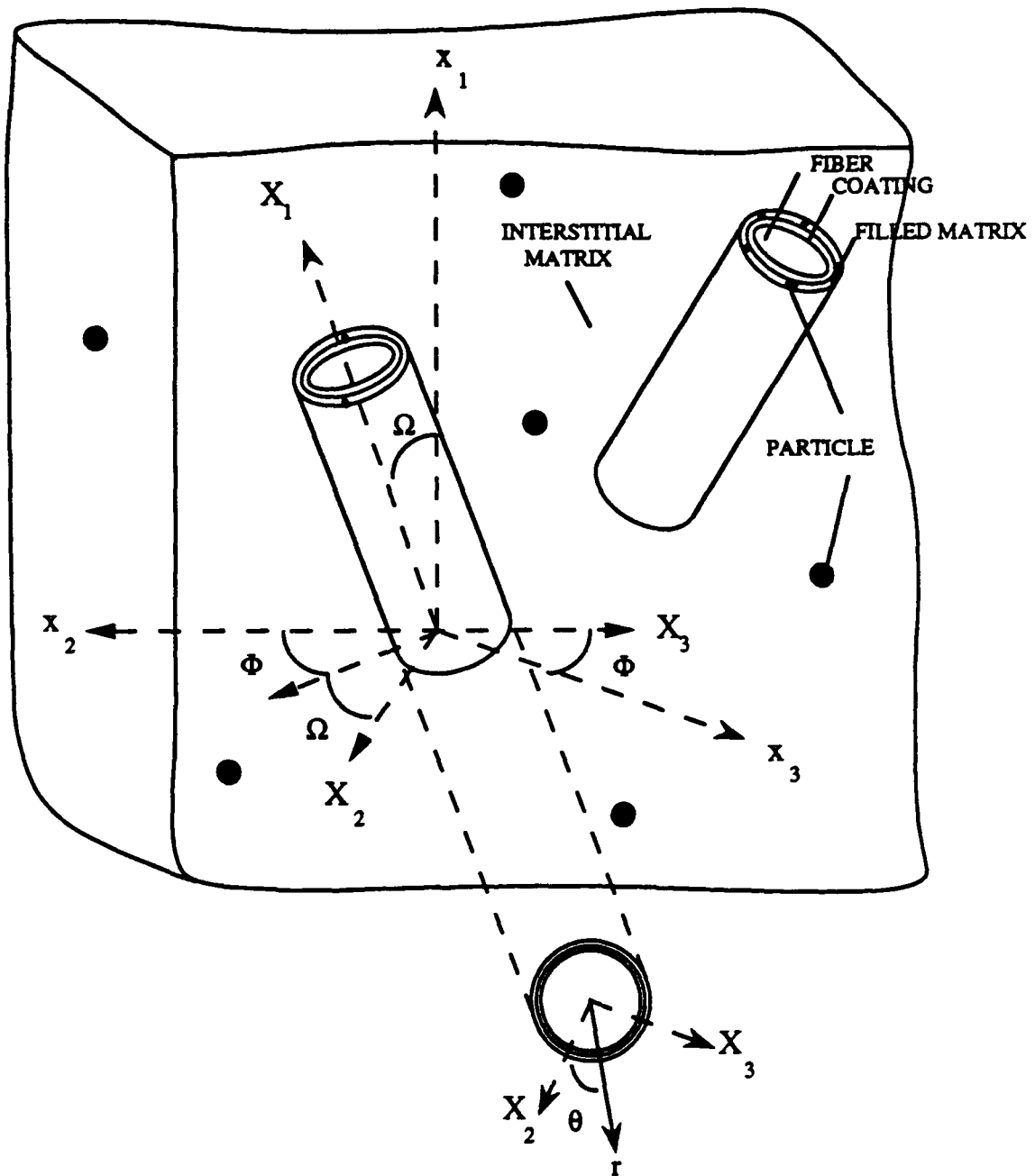


FIG 1. THEORETICAL MODEL

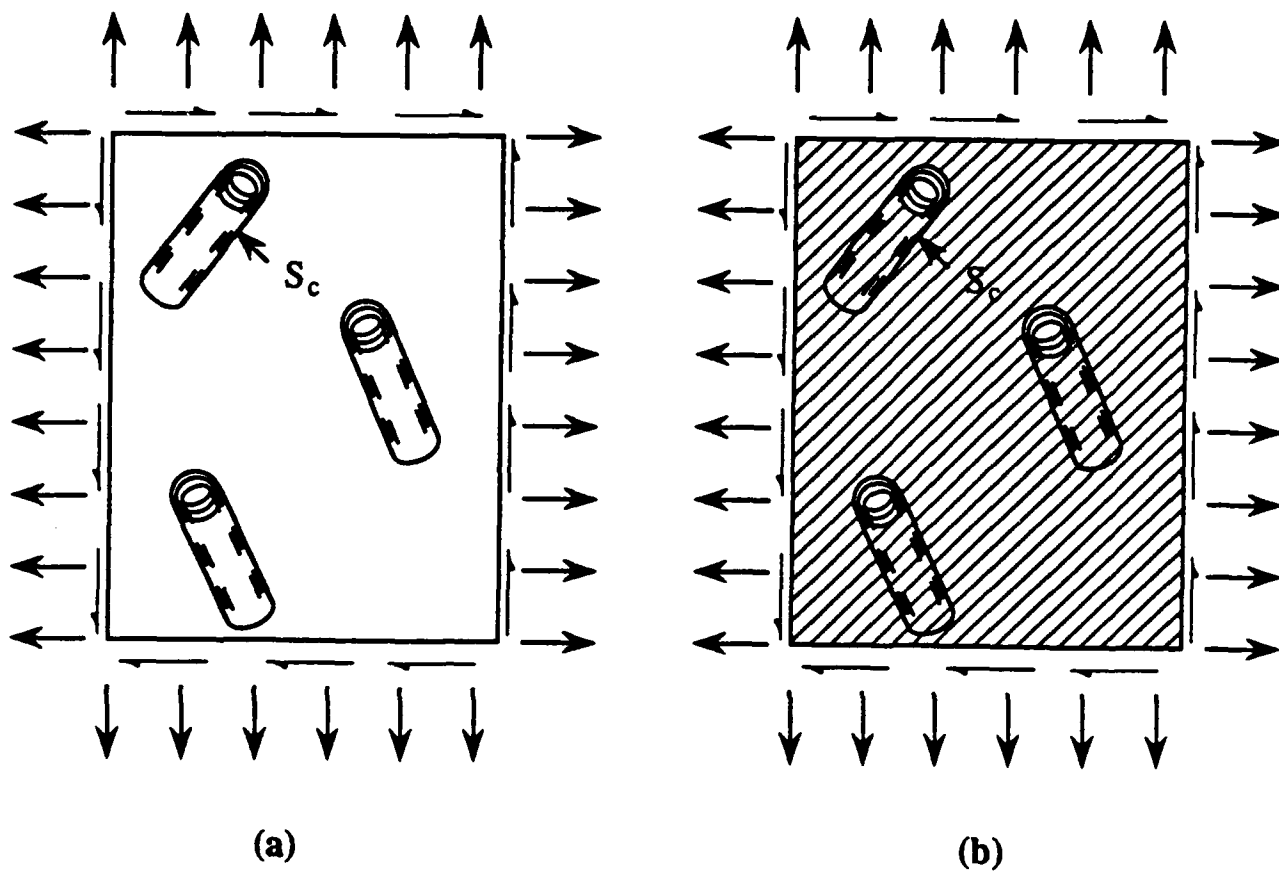
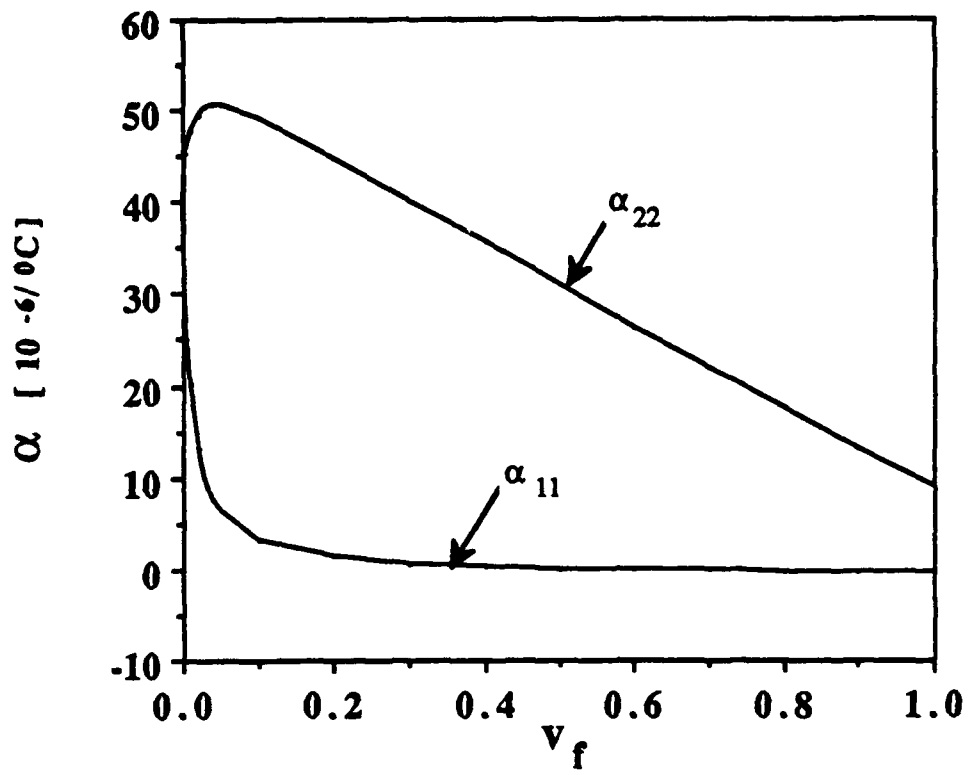
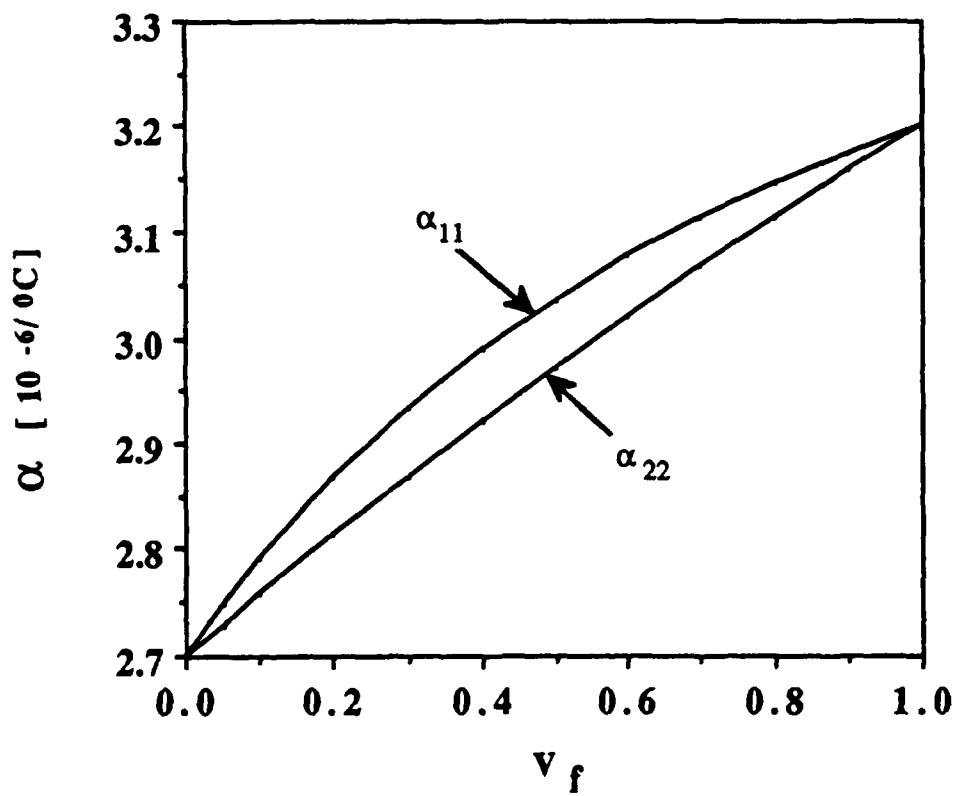


FIG 2. (a) COMPOSITE (b) EQUIVALENT HOMOGENEOUS BODY

**FIG 3. Effective thermal expansion coefficients for (a) Graphite/Epoxy system (b) Nicalon/BMAS system**



(a)



(b)

## **SECTION III**

### **CONSTRAINED MATRIX CRACKING**

## 1. INTRODUCTION

Ceramic matrix composites (CMC) generally exhibit weak fiber/matrix interfaces with very little or no chemical bonding. This has been shown to result in a considerable fracture toughness and the pronounced non-linearity in the load-elongation curve for a unidirectional CMC subjected to uniaxial tensile loading. The onset of the nonlinearity is associated with the widespread matrix cracking normal to the fibers and the applied load. The strain in the composite at matrix cracking may be higher than the failure strain of the matrix. If this matrix cracking strain can be increased it would be very beneficial in structural design. Wang [1], in his preliminary investigation alluded to the idea that having a strong bond between the matrix and the reinforcement (fiber) would enhance the matrix cracking strain. In this report an approximate analytical study is presented to show the effect of such interface constraint on matrix cracking.

The objectives of the study are:

1. To demonstrate analytically the effect of constraint on strain energy release rates and matrix cracking.
2. To propose an experimental scheme to show the effect of constraint.
3. To design a specimen to achieve the second objective.

## 2. ANALYTICAL MODEL

Isida [2] presented a theoretical analysis of the stress intensity factor for the tension of a centrally cracked strip reinforced with stringers along its edges as shown in Fig. 1. In the analysis both of the extensional rigidity and bending rigidity are taken into consideration. The analysis covers, as special cases, a centrally

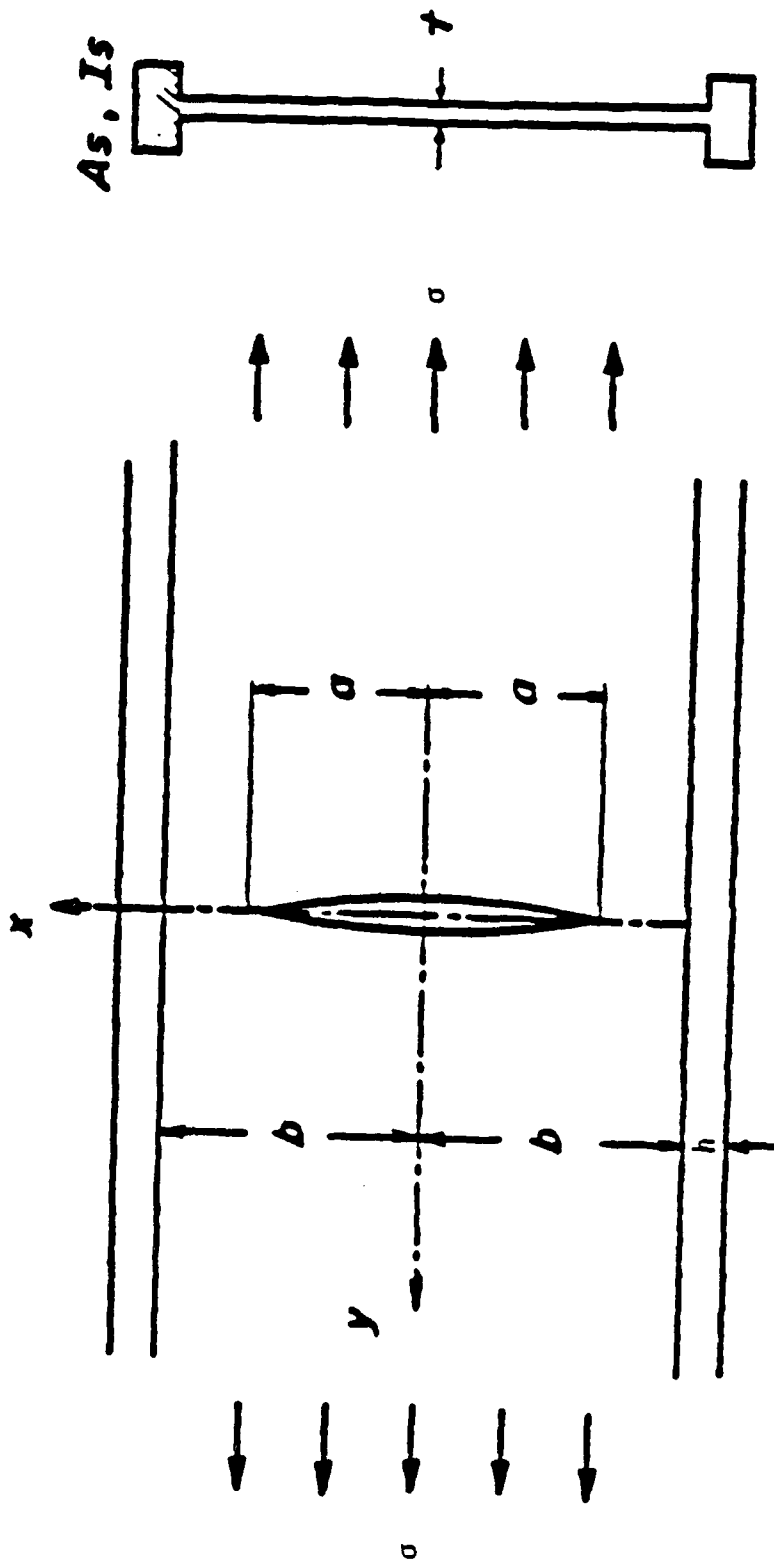


Fig. 1. Centrally cracked strip with stiffened edge (Isida, 1973).

cracked strip with free edges, that with clamped edges and a wide plate containing an infinite row of colinear cracks with and without parallel stringers between every adjacent cracks.

A transverse matrix crack in a unidirectional ceramic matrix composite with fibers parallel to the applied load is idealized and is assumed to be represented by a centrally cracked infinite strip reinforced with stringers along the both edges. The matrix is represented by the sheet and the fibers are presented by the stringers of appropriate stiffness. The idealized geometry is shown in Fig. 1.

Following Isida's [2] work, the stress intensity factor for the configuration shown in Fig. 1 is given by

$$K_I = \sigma \sqrt{\pi a} F(\alpha, \beta, \lambda) \quad (1)$$

where  $\sigma$  is the remote stress in the matrix,  $\alpha$  and  $\beta$  are the dimensionless inertia parameter and the dimensionless extensional rigidity of the individual stringers given by

$$\alpha = (E_s/E)(I_s/b^3t) \quad (2)$$

$$\beta = (E_s/E)(A_s/bt) \quad (3)$$

in which  $E_s$  is the Young's modulus of the stringers,  $E$  is the modulus of the matrix,  $I_s$  is the moment of inertia of the stringers and  $A_s$  is the sectional area of the stringers. The non-dimensional crack length  $\lambda$  is given by  $a/b$ . The correction factor  $F(\alpha, \beta, \lambda)$  is plotted for various combinations of  $\alpha$ ,  $\beta$  and  $\lambda$  in [2].

The strain energy release rate,  $G_I$ , for a crack completely in the matrix phase is given by

$$G_I = K_I^2/E \quad (4)$$

We assume that an existing flaw will grow when the strain energy release rate corresponding to that flaw size reaches or exceeds the

critical strain energy release rate for the matrix material,  $G_{IC}$ , that is

$$G_I = \sigma^2 \pi a [F(\alpha, \beta, \lambda)]^2 = G_{IC} \quad (5)$$

$$K_I = \sigma \sqrt{\pi a} F(\alpha, \beta, \lambda) = K_{IC} \quad (6)$$

From eq. (6), matrix cracking strain can be obtained the strain ( $\epsilon_{muc}$ ) as

$$\epsilon_{muc} = K_{IC} / [\sqrt{\pi a} E F(\alpha, \beta, \lambda)] \quad (7)$$

The cracking strain of the bulk matrix material stringers must be, however, equal to the ultimate failure strain of the brittle matrix material.

### 3. RESULTS AND DISCUSSION

In this section we present some typical results for a number of combinations of material pairings and crack dimensions in a normalized form as well as in terms of physical quantities. For the present study the stringers are assumed to be of width  $h$  and are of the same thickness ( $t$ ) as the sheet, so that the volume fraction of the stringers is given by

$$v_s = h/(h+b) \quad (8)$$

In Figs. 2 and 3 the normalized strain energy release rates are plotted as functions of stringer volume fraction for three stringer stiffnesses. Figure 2 corresponds to a moderate sized crack while Fig. 3 corresponds to a large crack. A decrease in the strain energy release rate indicates a decrease in the crack tip severity (intensity) and hence a less likelihood of crack propagation. This also reflects the so called pinning (clamping or constraint) effect on the crack tips provided by the stringers. For a given volume fraction the constraint is most effective for the highest stringer stiffness. For

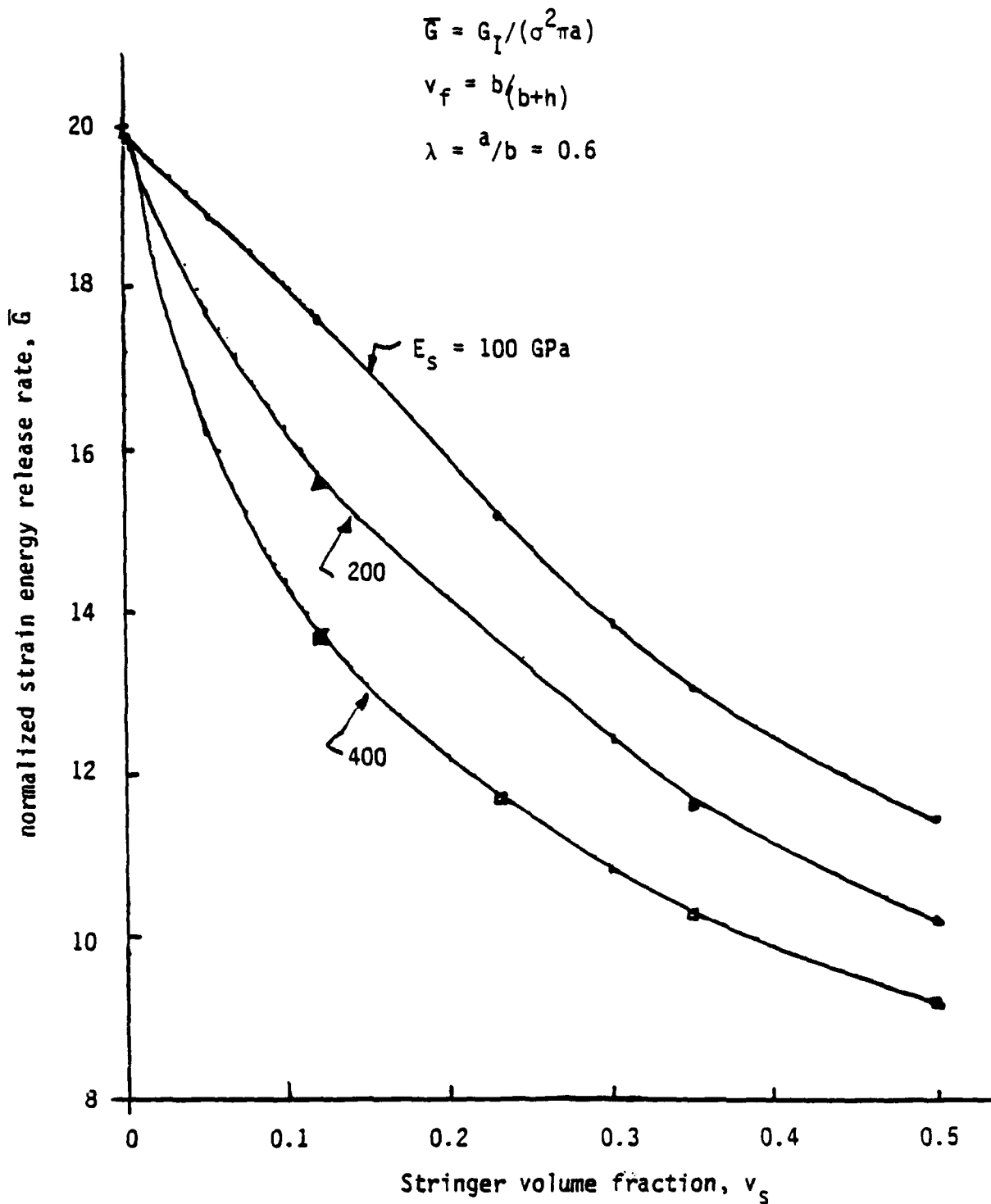


Fig. 2. Effect of stringers on strain energy release rate.

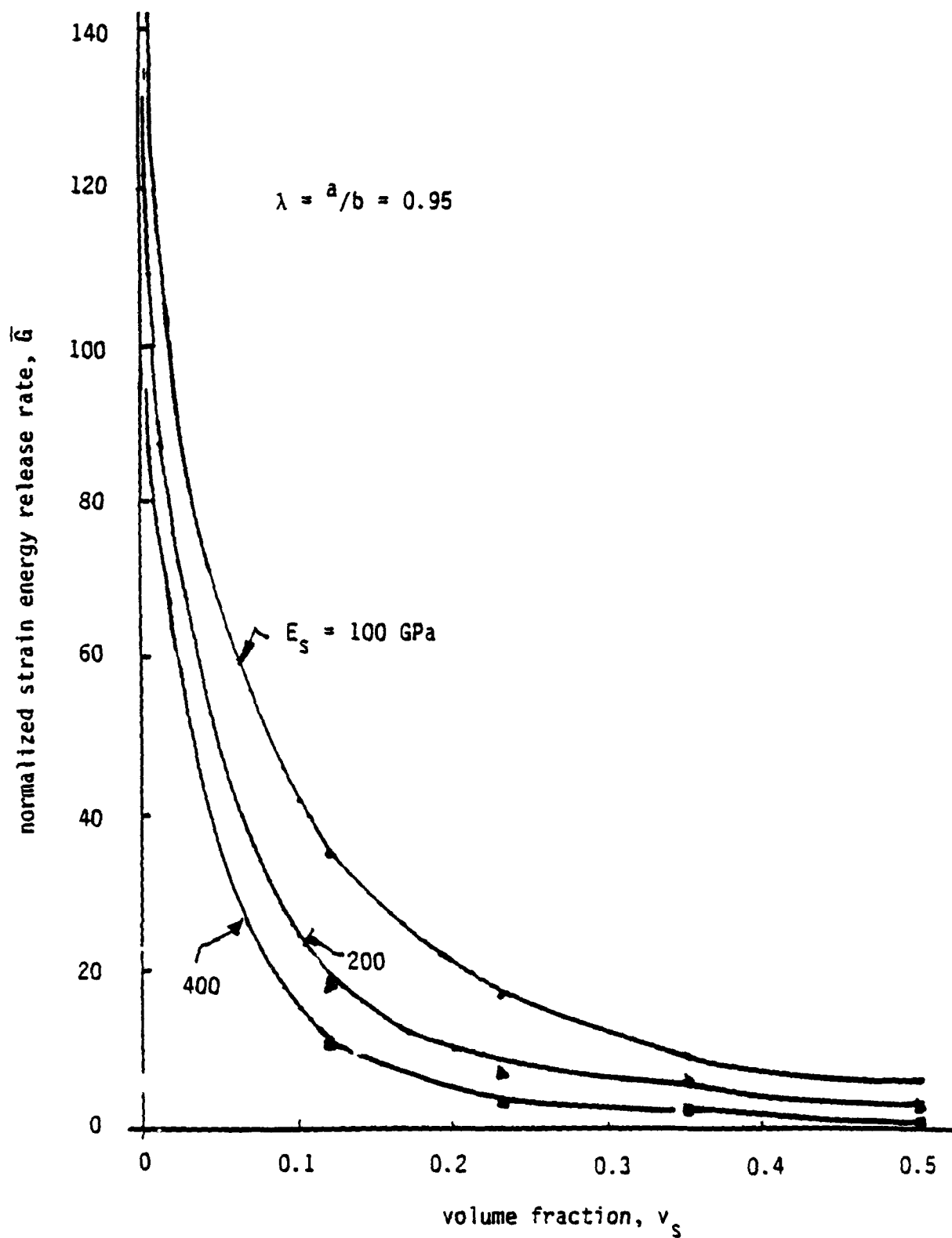


Fig. 3. Effect of stringers on strain energy release rate.

a given volume fraction of a particular stringer material the constraining effect is significantly higher when the crack tip is almost touching the stringers ( $\lambda = 0.95$ ). When the crack length is very small compared to the stringer spacing ( $2b$ ) the crack tip behaves as if in a monolithic matrix material. Next, we consider a particular material for the matrix, LAS, and illustrate the effect of constraint on the matrix cracking strain. Typically material properties of LAS are

$$E = 85 \text{ GPa}$$

$$\epsilon_{mu} \text{ (failure strain)} = 0.1\%$$

$$K_{Im} = 2 \text{ MPa}\sqrt{\text{m}}$$

From these properties we back calculate the inherent flaw size ( $a_0$ ) using the stress intensity factor for an infinite medium as

$$a_0 = K_{Ic} / (\sigma_{ult}^2) \quad (9)$$

where  $\sigma_{ult}$  is the ultimate strength of the matrix. Substitution of the appropriate values for the properties in eq. (9) results in  $a_0 = 0.1762 \text{ mm}$ .

In Fig. 4 the effect of stringer spacing on the growth of an inherent flaw is shown for a given stringer stiffness and various stringer sizes ( $h/b$ ). It takes a significantly higher strain to propagate an inherent flaw when the stringer spacing is of the order of crack size and as stringer spacing increases the cracking strain approaches that of monolithic matrix material. The same conclusions can be drawn by looking at the stresses required to propagate an inherent flaw shown in Fig. 5 for a given stringer size ( $h = 0.15 \text{ mm}$ ) and three different stringer stiffnesses.

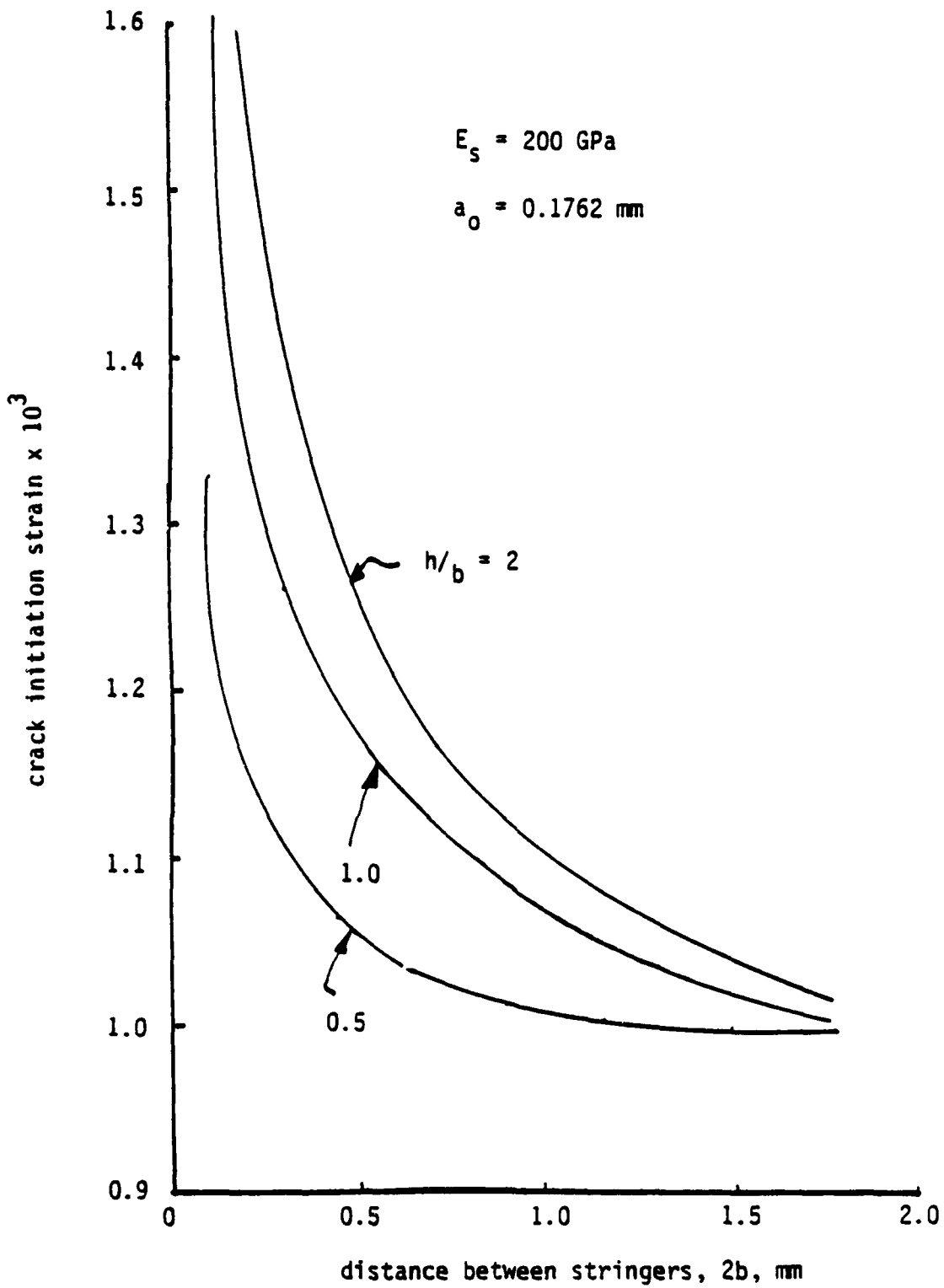


Fig. 4. Effect of stringer size on inherent flaw growth

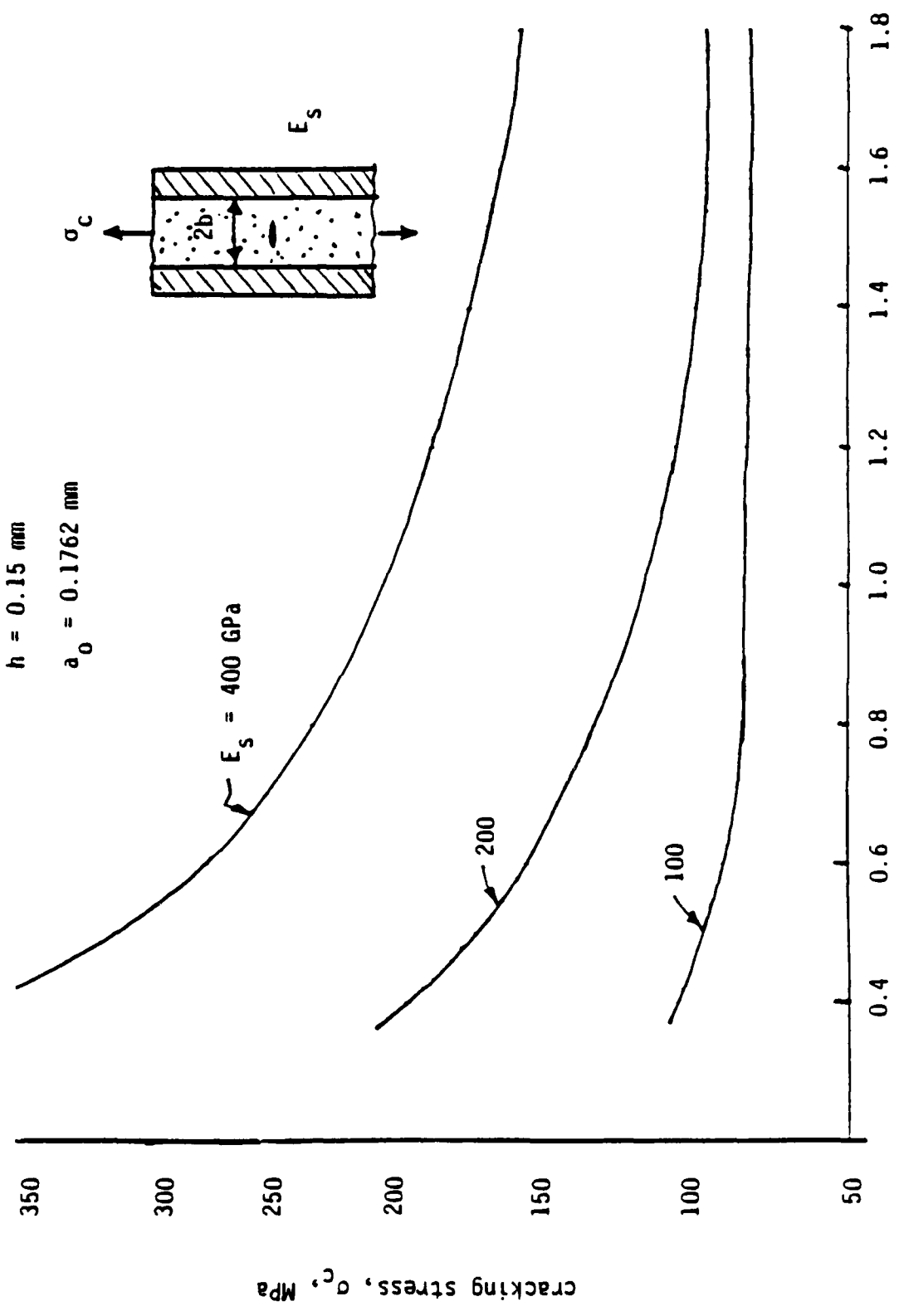


Fig. 5. Matrix cracking stress

Since the stress intensity factor decreases as the crack propagates towards a stringer, it is likely that the inherent flaw once initiated may not grow unstably if the remote strain held constant. The solid line in Figs. 6-8 represents the strain for initiation (onset of growth of an inherent flaw) and the broken line represents the strain for the crack to grow upto the matrix-stringer interface ( $a/b = 0.95$ ). We will take the strain corresponding to the solid line as the "constrained matrix cracking strain" and assume the cracks at this strain are observable in an experiment. The cross over point (A) in these figures indicates that the constraint effect of the stringers is zero for spacing larger than  $b_A$ . This critical stringer spacing ( $b_A$ ) is strongly dependent on the stringer stiffness, that is, for  $E_S = 100$ ,  $b_A = 0.4$  mm, for  $E_S = 200$ ,  $b_A = 0.63$  mm, and for  $E_S = 400$ ,  $b_A$  is very large. This is a significant observation in that if this logic is extended to CMC materials it is reasonable to believe that for a given fiber-matrix system there is a critical fiber spacing beyond which there is no further increase in the cracking strain of the composite.

In Fig. 9 we present failure strain (constrained matrix cracking strain) as a function of stiffener thickness for two matrix layer thicknesses. For the stiffener material, two systems are considered; Avco fiber/LAS matrix and Nicalon fiber/LAS matrix both 50% volume fraction. Results of Fig. 9 can be used in the design of a test specimen for studying the constraint effect experimentally.

Finally, an approximate design guide line is presented for the experimental part of this investigation. Three possible stringer materials are 50% volume fraction Nicalon/LAS, Avco/LAS and Graphite/Epoxy unidirectional composites with fibers parallel to the loading.

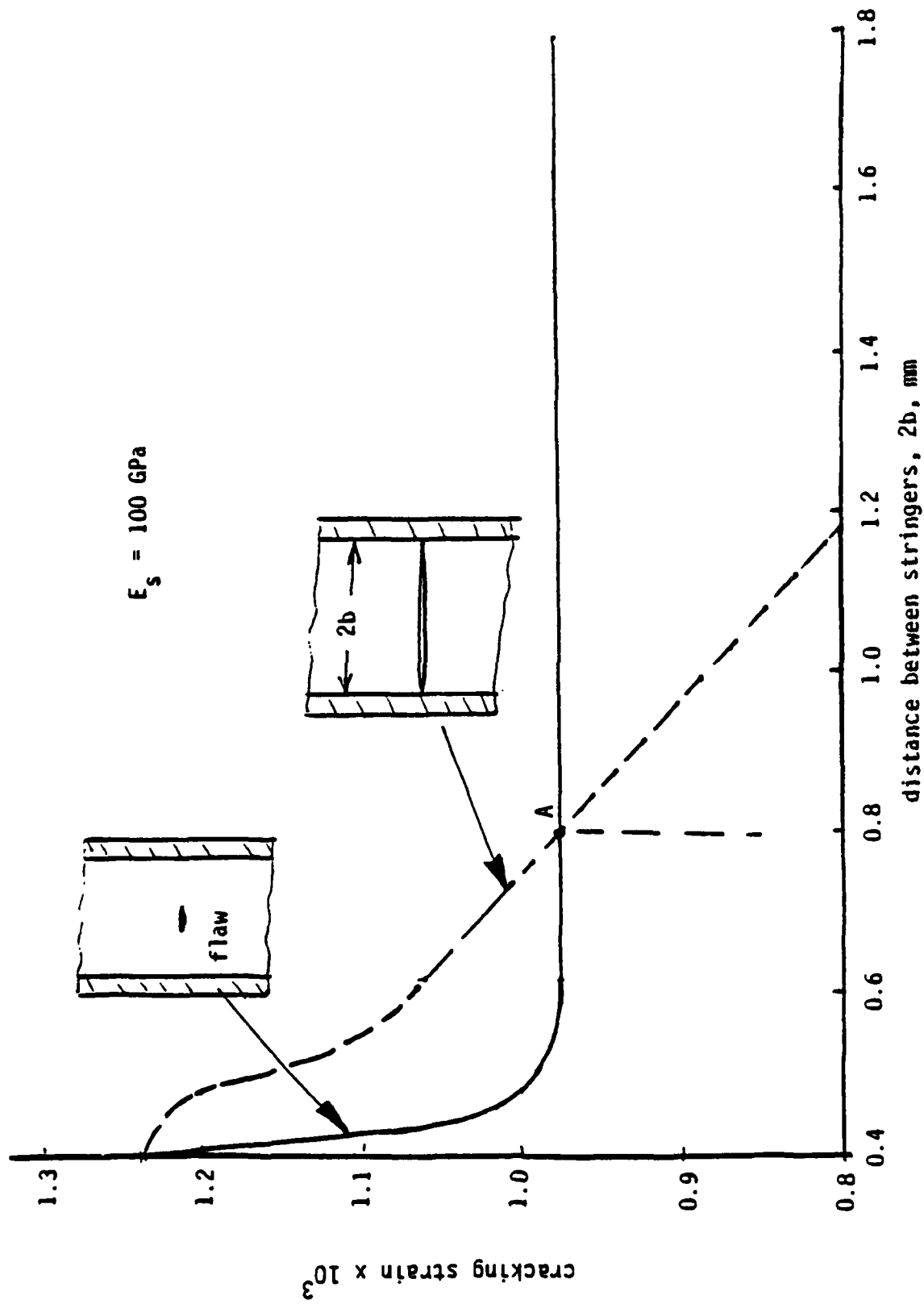


Fig. 6. Effect of spacing on crack initiation and growth

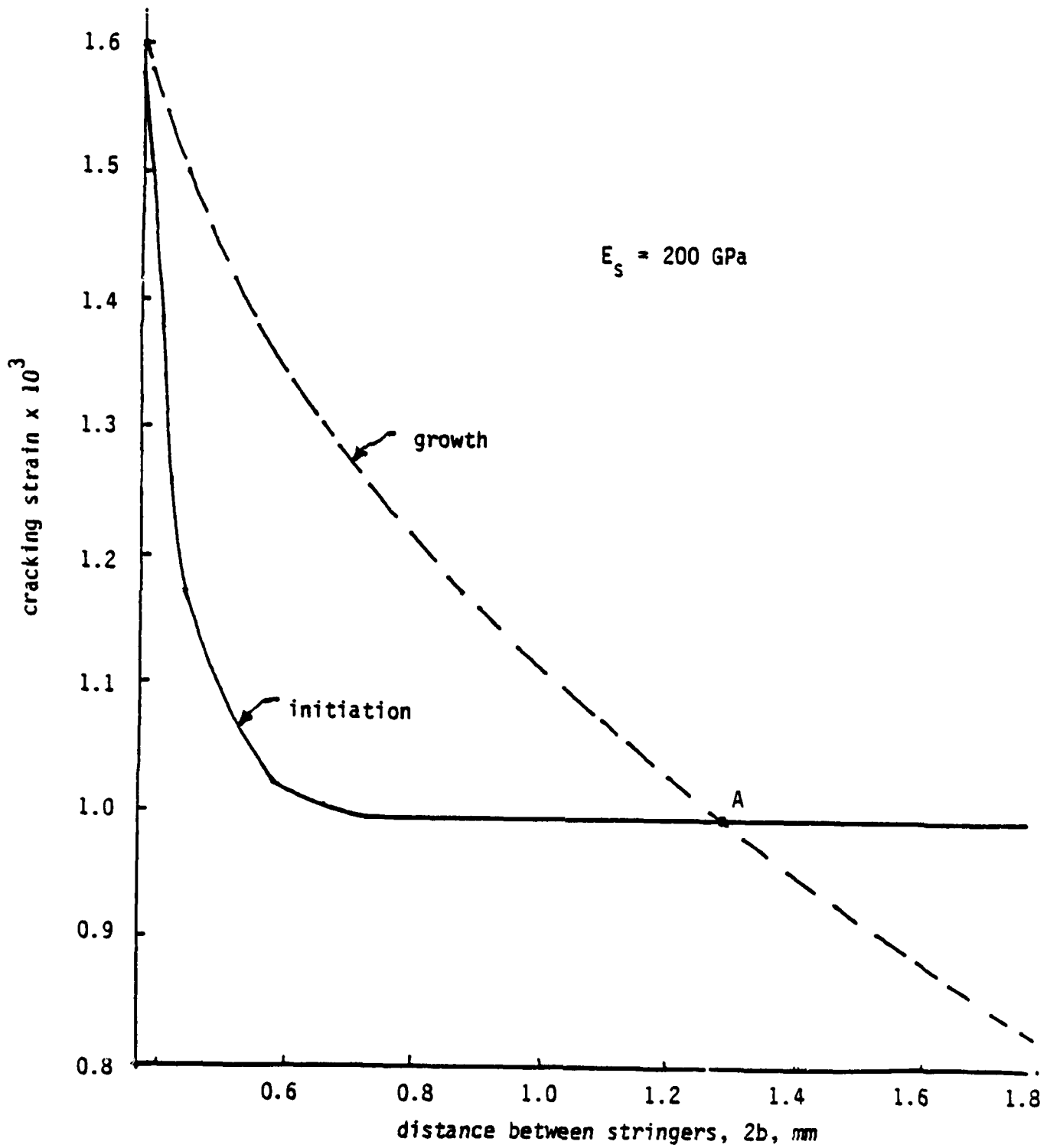


Fig. 7. Effect of spacing on crack initiation and growth

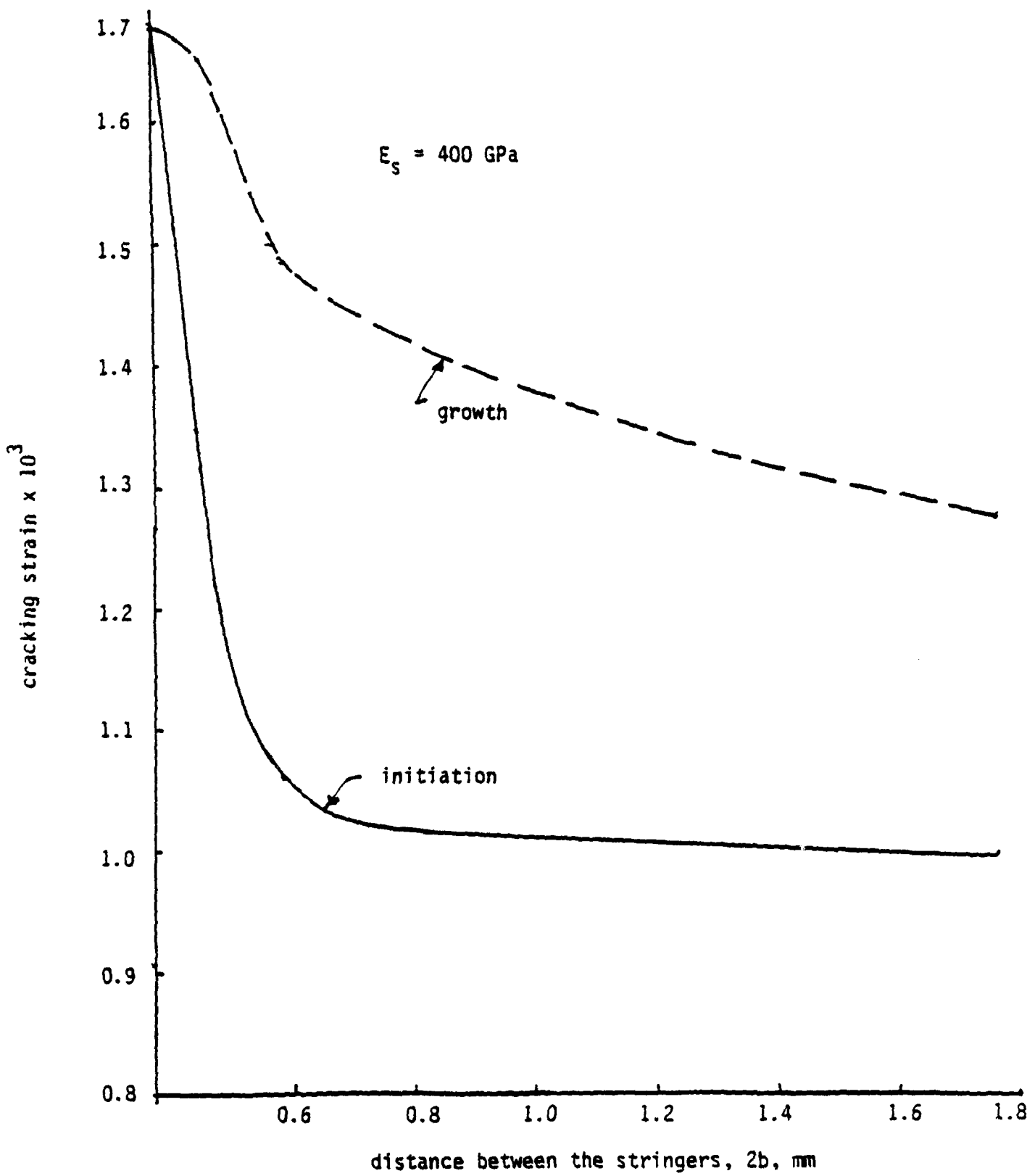


Fig. 8. Effect of spacing on crack initiation and growth

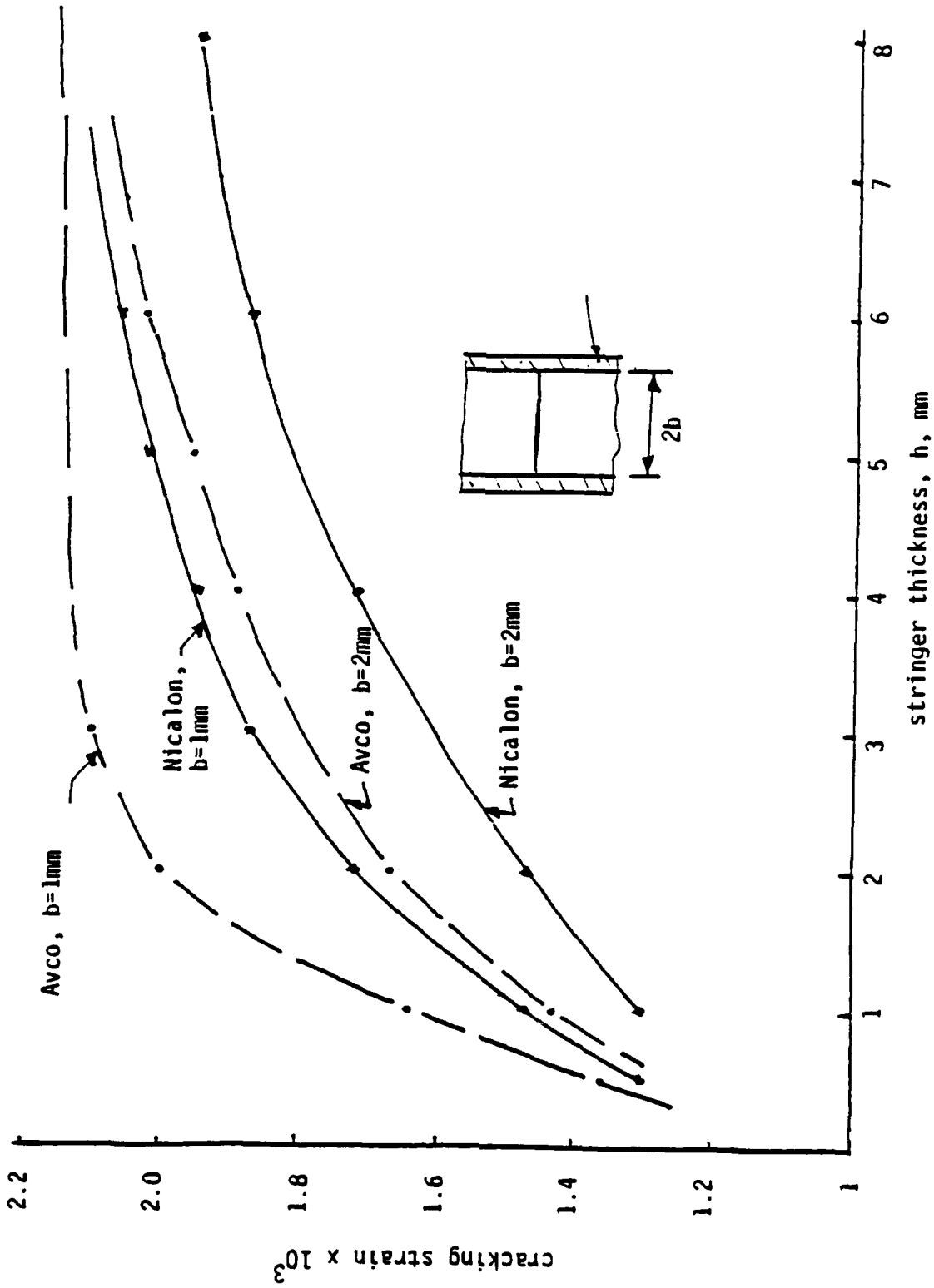


Fig. 9. Effect of stringer thickness on cracking strain

Approximate dimensions required to double the matrix failure strain, 0.1% to 0.2%, and the corresponding predicted loads at this cracking strain are presented in Table I. The load ranges are large enough that a conventional uniaxial tensile test can be performed on these specimens and the cracks can be observed by coating the specimen edges with a white paint. It is conceivable that the onset of cracking may not result in a noticeable drop in load-elongation plot.

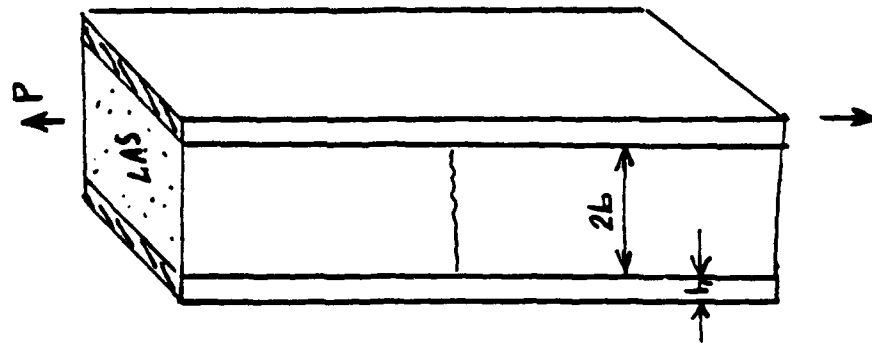
#### 4. CONCLUSIONS

The foregoing results show that the constraint provided by the stringers which are fully bonded to the matrix will enhance the matrix cracking strain. It does not, however, mean that the composite would be tougher. We have not considered the effects due to material orthotropy, stringer failure, the interface failure and the periodic spacing of the fibers in the above study.

#### REFERENCES

1. A. S. D. Wang, "On Some Basic Concepts of Failure in BMC," Seminar Notes, AFWAL, WPAFB, May 26, 1988.
2. M. Isida, "Analysis of Stress Intensity Factors for the Tension of a Centrally Cracked Strip with Stiffened Strips," Engineering Fracture Mechanics, Vol. 5, pp. 647-665, 1973.
3. D. Broek, "Elementary Engineering Fracture Mechanics," Martinus Nijhoff Publishers, The Hague, 1983.

Table 1. Specimen Dimensions for Doubling the Failure Strain



Constr.	2b(mm)	h(mm)	P <sub>cr</sub> * (kn)
Nicalon/ Las	2	4.7	30.2
	4	9	58.1
Avco/Las	2	2	23.2
	4	5.8	64.2
Graphite/ Epoxy	2	3.4	28.2
	4	7.2	59.2

\*P<sub>cr</sub> matrix cracking load